

SLAC - PUB - 4370 Rev.
January 1988
(A)

SUPERCONVERGENT TRACKING*

TOR O. RAUBENHEIMER AND RONALD D. RUTH

*Stanford Linear Accelerator Center
Stanford University, Stanford, California, 94305*

ABSTRACT

In this paper we develop a new technique (superconvergent tracking) for tracking particles through a circular accelerator or a transport line with nonlinear elements. We use the superconvergent perturbation theory of Kolmogorov to solve the Hamilton-Jacobi equation (approximately) over a finite time interval. This transformation defines a map from the initial conditions to the state of the system at some later time. This technique can be iterated to examine long term stability in betatron phase space in a circular accelerator or it can be used to calculate the trajectory in betatron phase space of particles in a transport line. We verify the algorithm with two test cases in one degree of freedom, and then further develop the technique to track the two transverse degrees of freedom in a general accelerator lattice with sextupoles. As an example we track a section of the SSC arcs with and without sextupole errors in the bending magnets.

Submitted to *Particle Accelerators*

* Work supported by the Department of Energy, contract DE-AC03-76SF00515

1. INTRODUCTION

The purpose of this paper is to explore a new algorithm for computing the trajectory of a particle in a circular accelerator or transport line. Presently, there exist many different techniques for 'tracking' a particle or a collection of particles through an accelerator 'lattice' (the collection of dipoles, quadrupoles, sextupoles, *etc.* which are used to guide the particle and maintain transverse stability).¹⁻³ Each of these techniques has its strengths and weaknesses.

The basic problem is a trade off between accuracy and speed. In the extreme case one can simply numerically integrate the differential equations through each magnetic element. This of course is extremely slow and in practice is not used at all in the study of 'long term' stability in storage rings. On the other hand this careful but slow method is useful for studying finite length transport lines in which nonlinear effects are important, for example the transport and final focus of a linear collider. However, even in this case numerical integration suffers in that it gives little insight into the design problem of aberration-free final focus systems.

The other extreme is the study of long-term stability in storage rings. In this case one would like to examine the stability for hours in the case of protons or for a few radiation damping times in the case of electrons. In practice, however, one is limited to about an hour of *calculation* time with the tracking technique being used. Therefore, the tracking times usually fall far short of the ultimate goal.

To study long term stability it is therefore useful to augment the numerical techniques for orbit study with analytic techniques. Perhaps one should say that the numerical techniques augment the analytic techniques! The problem of

interest is the long term stability of a weakly nonlinear system which has two transverse degrees of freedom (and possibly the longitudinal degree of freedom as well) with forcing terms that are functions of the independent variable. This yields a Hamiltonian which is a function of the two coordinates, their canonical momenta and the independent variable, s . This is sometimes referred to as a system with $2\frac{1}{2}$ degrees of freedom. There are many new techniques for studying this problem and also some useful old techniques. For a review of various techniques used in the study of nonlinear dynamics see Ref. 4.

In this paper we are concerned with tracking techniques which use methods that are borrowed from the analytic and perturbative study of stability. The basic idea is taken from canonical perturbation theory⁴ which has its roots in Hamilton-Jacobi theory. In the Hamilton-Jacobi approach one attempts to find a canonical transformation of the coordinates and momenta which converts the problem to one where the Hamiltonian is a function only of the new momenta. Since this new problem is trivial to solve (the new momenta are the constants of the motion), all of the dynamics is wrapped up in the canonical transformation. This technique can be applied as one of the analytic tools to study long term stability.⁵

In the present case we apply this technique to the particle orbit. The idea is to find a canonical transformation which will leave the new Hamiltonian a linear function of the momentum. In such a case the new momenta is a constant of the motion while the new coordinates are simple functions of the independent variable, and thus with appropriate boundary conditions on the canonical transformation the new momentum can be taken to be an initial condition. Thus the canonical transformation defines a map from the present state of the system

to the initial conditions. If this map is inverted, it yields a map of the initial conditions to the present state of the system. In this paper we find this desired canonical transformation perturbatively using the techniques of canonical perturbation theory. This yields an analytic representation of the map which can then be iterated numerically to study long term stability.

The map obtained using this technique will differ slightly from those found using other techniques in that the expansion is made treating the perturbation or multipole strength as the small parameter. Matrix methods such as TRANSPORT⁶ expand in a Taylor series about a trajectory, treating \vec{x} as the small parameter while integration techniques such as symplectic integration⁷ expand in terms of the distance travelled through the magnets.

In Section 2 we begin by calculating the generating function as an iteration of superconvergent perturbation theory. We carry this forward analytically through two steps of the process. In Section 3 we demonstrate the technique by using the 'superconvergent tracking'⁸ algorithm on two model problems in one degree of freedom. These serve to illustrate the salient features and are not unlike many problems in accelerators. In Section 4 we develop the technique for a general accelerator lattice with an arbitrary sextupole distribution. Finally, in the last section we treat several model lattices taken from the design study for the SSC.

2. SUPERCONVERGENT TRACKING

The aim of superconvergent tracking is to calculate a map which takes the initial conditions at one point in a magnetic lattice to final conditions at some other point. For a circular accelerator or storage ring, one would like to calculate the map for a significant fraction of an entire turn. Once this map is obtained, it can be iterated numerically to discover long term behavior.

The map is generated by a sequence of canonical transformations so that after n steps the Hamiltonian is a linear function of the new momentum through some order in the perturbation strength. In such a case, the new momentum is constant and the new position is a constant plus a phase which advances with the independent variable. Thus with the appropriate boundary conditions on the generating function, the new momentum and the new position minus the phase advance can be used as initial conditions. The map is then obtained by applying the transformations in reverse order. This, in effect, solves the Hamiltonian-Jacobi equation for a finite interval in the independent variable.

We begin with the Hamiltonian for linear motion perturbed by V_0 , a small nonlinear term of order ϵ ,

$$H_0 = \boldsymbol{\nu} \cdot \mathbf{J}_0 + V_0(\boldsymbol{\phi}_0, \mathbf{J}_0, \theta) \quad (2.1)$$

where V_0 is periodic in both $\boldsymbol{\phi}_0$ and θ . Note that throughout this paper bold face characters denote d-dimensional vectors and variables will be used as subscripts to indicate partial differentiation.

Now we perform the first of a sequence of canonical transformations with the

generating function⁹

$$F_2(\phi_0, \mathbf{J}_1, \theta) = \phi_0 \cdot \mathbf{J}_1 + G^{(1)}(\phi_0, \mathbf{J}_1, \theta) , \quad (2.2)$$

which yields the transformation equations

$$\begin{aligned} \mathbf{J}_0 &= \mathbf{J}_1 + G_{\phi_0}^{(1)}(\phi_0, \mathbf{J}_1, \theta) \\ \phi_1 &= \phi_0 + G_{\mathbf{J}_1}^{(1)}(\phi_0, \mathbf{J}_1, \theta) , \end{aligned} \quad (2.3)$$

and the new Hamiltonian

$$H_1 = \nu \cdot \mathbf{J}_1 + \nu \cdot G_{\phi_0}^{(1)} + V_0(\phi_0, \mathbf{J}_1 + G_{\phi_0}^{(1)}, \theta) + G_{\theta}^{(1)} . \quad (2.4)$$

This in turn can be written in the suggestive form

$$\begin{aligned} H_1 &= \nu \cdot \mathbf{J}_1 + V_0(\phi_0, \mathbf{J}_1 + G_{\phi_0}^{(1)}, \theta) - V_0(\phi_0, \mathbf{J}_1, \theta) \\ &+ \left[G_{\theta}^{(1)} + \nu \cdot G_{\phi_0}^{(1)} + V_0(\phi_0, \mathbf{J}_1, \theta) \right] . \end{aligned} \quad (2.5)$$

Note that the Hamiltonian has temporarily been left in the same mixed variables as $G^{(1)}$.

We would like to find $G^{(1)}$ so that the perturbation in H_1 is higher order in the perturbation strength. If we solve for $G^{(1)}$ such that the bracket in Eq. (2.5) is zero, then the new Hamiltonian is a linear function of \mathbf{J}_1 plus a perturbation of order ϵ^2 . Completing the substitution, we are left with

$$H_1(\phi_1, \mathbf{J}_1, \theta) = \nu \cdot \mathbf{J}_1 + V_1(\phi_1, \mathbf{J}_1, \theta) \quad (2.6)$$

where

$$V_1(\phi_1, \mathbf{J}_1, \theta) \equiv V_0(\phi_0, \mathbf{J}_1 + G_{\phi_0}^{(1)}, \theta) - V_0(\phi_0, \mathbf{J}_1, \theta) , \quad (2.7)$$

and where ϕ_0 will be expressed as a function of ϕ_1 , \mathbf{J}_1 , and θ by inverting (2.3). It is easy to see that V_1 is of order ϵ^2 by expanding V_0 about \mathbf{J}_1 for small $G_{\phi_0}^{(1)}$.

At this point we can return to Eqs. (2.3) to repeat the process. Stopping after n steps, we find

$$\begin{aligned} H_n &= \nu \cdot \mathbf{J}_n + V_n(\phi_n, \mathbf{J}_n, \theta) \\ V_n &\sim O(\epsilon^{2^n}), \end{aligned} \quad (2.8)$$

and from Hamilton's equations

$$\begin{aligned} \phi_n &= \nu\theta + \text{constant} + O(\epsilon^{2^n}) \\ \mathbf{J}_n &= \text{constant} + O(\epsilon^{2^n}). \end{aligned} \quad (2.9)$$

Thus, provided that ϵ is sufficiently small, \mathbf{J}_n is constant while ϕ_n advances uniformly in θ .

As an illustration of the technique we will calculate the second order transformation in one dimension for an arbitrary non-linear perturbation V_0 . By expressing $G^{(1)}$ and V_0 as a Fourier series in ϕ_0 , the bracket in Eq. (2.5) becomes

$$\frac{\partial g_m(J_1, \theta)}{\partial \theta} + im\nu g_m(J_1, \theta) = -v_m(J_1, \theta), \quad (2.10)$$

where g_m and v_m are the Fourier coefficients for $G^{(1)}$ and V_0 respectively. The first order differential equation requires a boundary condition to specify the unique solution. The condition we impose is that $G^{(1)} \rightarrow 0$ as $\theta_f \rightarrow \theta_i$, *i.e.* the canonical transform becomes the identity transform when $\theta_f = \theta_i$. Thus (ϕ_1, J_1) will equal (ϕ_0, J_0) at $\theta_f = \theta_i$. The solution for $G^{(1)}$ is then

$$G^{(1)}(\phi_0, J_1, \theta_f, \theta_i) = - \sum_m e^{im\phi_0} \int_{\theta_i}^{\theta_f} v_m(J_1, \theta') e^{im\nu(\theta' - \theta_f)} d\theta'. \quad (2.11)$$

Although $G^{(1)}$ is not a periodic function of θ , it is important to note that since V_0 is periodic in θ , $G^{(1)}$ is invariant if both θ_i and θ_f are shifted by 2π .

The form of the new Hamiltonian is shown in Eq. (2.6). Before the second transformation can be calculated, V_1 from Eq. (2.7) must be re-written in terms of the new variables, ϕ_1 and J_1 . To do so, we expand $V_0(\phi_0, J_1 + G_{\phi_0}^{(1)}, \theta)$ and $G_{\phi_0}^{(1)}$ in Taylor series:

$$\begin{aligned} V_1(\phi_1, J_1, \theta) &= V_{J_1}(\phi_0, J_1, \theta)G_{\phi_0}(\phi_0, J_1, \theta) + V_{J_1 J_1} \frac{G_{\phi_0}^2}{2} + \dots \\ G_{\phi_0}(\phi_0, J_1, \theta) &= G_{\phi_1}(\phi_1, J_1, \theta) + \Delta\phi G_{\phi_1 \phi_1} + \dots \\ V(\phi_0, J_1, \theta) &= V(\phi_1, J_1, \theta) + \Delta\phi V_{\phi_1} + \dots \end{aligned} \quad (2.12)$$

where $\Delta\phi = \phi_0 - \phi_1$. Note that the sub/superscripts on V_0 and $G^{(1)}$ have been dropped for simplicity. Now $\Delta\phi$ is calculated from Eqs. (2.3)

$$\Delta\phi = -[G_{J_1}(\phi_1, J_1, \theta) + G_{J_1 \phi_1} G_{J_1} + \dots].$$

We then combine the equations, keeping only terms through order ϵ^3 since H_2 , and therefore the error, will be of order ϵ^4 :

$$H_1 = \nu J_1 + V_1(\phi_1, J_1, \theta) \quad (2.13)$$

where

$$\begin{aligned} V_1(\phi_1, J_1, \theta) &= V_{J_1} G_{\phi_1} + \frac{1}{2} V_{J_1 J_1} G_{\phi_1}^2 \\ &\quad - V_{J_1 \phi_1} G_{\phi_1} G_{J_1} - V_{J_1} G_{\phi_1 \phi_1} G_{J_1} + O(\epsilon^4). \end{aligned} \quad (2.14)$$

Finally, $G^{(2)}$ is calculated from V_1 in a manner identical to that of $G^{(1)}$,

$$G^{(2)}(\phi_1, J_2, \theta_f) = - \sum_m e^{im\phi_1} \int_{\theta_i}^{\theta_f} v_{1m}(J_2, \theta') e^{im\nu(\theta' - \theta_f)} d\theta' \quad (2.15)$$

where v_{1m} are the Fourier coefficients of V_1 . Again note that $G^{(2)}$ is invariant if both θ_f and θ_i are incremented by 2π .

When tracking we find a particle's position, in phase space, from a prior position; we need to calculate $(\phi_0, \mathbf{J}_0)_{\theta=\theta_f}$ given $(\phi_0, \mathbf{J}_0)_{\theta=\theta_i}$. Using Hamilton's equations, Eqs. (2.9), and knowledge of the boundary condition on the generating functions, we can easily estimate $(\phi_n, \mathbf{J}_n)_{\theta=\theta_f}$ from the initial conditions:

$$\begin{aligned}\phi_{n\theta=\theta_f} &= \phi_i + \nu(\theta_f - \theta_i) + O(\epsilon^{2^n}) \\ \mathbf{J}_{n\theta=\theta_f} &= \mathbf{J}_i + O(\epsilon^{2^n}).\end{aligned}\tag{2.16}$$

Now by inverting the canonical transformations, Eqs. (2.3), we can calculate (ϕ_0, \mathbf{J}_0) from (ϕ_n, \mathbf{J}_n) . First we solve for ϕ_{n-1} implicitly and then we can calculate \mathbf{J}_{n-1} explicitly

$$\begin{aligned}\phi_{n-1\theta=\theta_f} &= \phi_{n\theta=\theta_f} - G_{\mathbf{J}_1}^{(n)}(\phi_{n-1}, \mathbf{J}_n, \theta_f) \\ \mathbf{J}_{n-1\theta=\theta_f} &= \mathbf{J}_{n\theta=\theta_f} + G_{\phi_0}^{(n)}(\phi_{n-1}, \mathbf{J}_n, \theta_f).\end{aligned}\tag{2.17}$$

In this manner we reverse each transform until we arrive at the values of ϕ_0 and \mathbf{J}_0 . The error of $(\phi_0, \mathbf{J}_0)_{\theta=\theta_f}$ is then of the same order as the error in $(\phi_n, \mathbf{J}_n)_{\theta=\theta_f}$.

The tracking algorithm will approximate the true motion only if the strength of the perturbation, ϵ , is small. In addition it is necessary to control the step size $\theta_f - \theta_i \equiv \Delta\theta$. Assuming that the perturbation varies slowly with θ , $G^{(1)}$, shown in Eq. (2.11), will be linear in $\Delta\theta$ for small $\Delta\theta$. Additionally, if $G^{(1)}$ has terms with $m = 0$, true for octupole perturbations but not for sextupoles, then these terms will be linear in $\Delta\theta$. The $\Delta\theta$ terms will then appear in V_1 through the partial derivatives of $G^{(1)}$ with respect to \mathbf{J}_1 , upon which V_1 is linearly dependent. Therefore V_1 will also be linear in $\Delta\theta$. Now looking at Hamilton's equations for \mathbf{J}_1 and ϕ_1 we can see that the error will be of order $\Delta\theta^2$ for one step since V_1 is

integrated over the range $\Delta\theta$,

$$\begin{aligned} \mathbf{J}_1 &= - \int_{\theta_i}^{\theta_f} \frac{\partial H_1}{\partial \phi_1} d\theta = \mathbf{J}_i + O(\Delta\theta^2) && \text{(one step)} \\ \phi_1 &= \int_{\theta_i}^{\theta_f} \frac{\partial H_1}{\partial \mathbf{J}_1} d\theta = \phi_i + \nu(\theta_f - \theta_i) + O(\Delta\theta^2) . && \text{(one step)} \end{aligned} \tag{2.18}$$

Since we are actually interested in the error over one turn which is composed of N steps of length $\Delta\theta$, the error in \mathbf{J}_1 and ϕ_1 will depend linearly upon $\Delta\theta$

$$\begin{aligned} \mathbf{J}_1 &= \mathbf{J}_i + O(\Delta\theta) && \text{(one turn)} \\ \phi_1 &= \phi_i + \nu(\theta_f - \theta_i) + O(\Delta\theta) . && \text{(one turn)} \end{aligned} \tag{2.19}$$

Similarly, terms in $G^{(2)}$ will increase quadratically with $\Delta\theta$ since V_1 is linear in $\Delta\theta$. H_2 will then depend cubically upon $\Delta\theta$, and thus the error of (ϕ_2, \mathbf{J}_2) will also increase cubically with $\Delta\theta$

$$\begin{aligned} \mathbf{J}_2 &= \mathbf{J}_i + O(\Delta\theta^3) && \text{(one turn)} \\ \phi_2 &= \phi_i + \nu(\theta_f - \theta_i) + O(\Delta\theta^3) . && \text{(one turn)} \end{aligned} \tag{2.20}$$

This dependence is important since it restricts the distance over which we can track while maintaining accuracy, and thereby may force us to divide the ring into steps. It also allows us to check the convergence of the algorithm by changing the step size and comparing results, much like an adaptive quadrature routine. When the errors obey the power law dependance on $\Delta\theta$, *i.e.* when the perturbation varies slowly with θ , the error for the second order tracking can be written

$$(f_1 - f_{true}) = \alpha\theta^3 , \quad \alpha = \frac{f_1 - f_2}{\theta_1^3 - \theta_2^3} , \tag{2.21}$$

where f_{true} , f_1 , and f_2 are values of $J_{x,y}$ or $\phi_{x,y}$ for the exact solution and tracking with steps of θ_1 and θ_2 respectively.

3. TRACKING IN ONE DEGREE OF FREEDOM

In this section the superconvergent tracking algorithm is tested on two simple problems with one degree of freedom (and a time dependent Hamiltonian). In the first case (i) we examine a sextupole perturbation whose strength varies as $\cos(\theta)$, and in the second case (ii) a periodic delta function octupole perturbation. In both cases we use a smooth approximation for the focusing in the ring so the unperturbed motion is a simple harmonic oscillation. The Hamiltonians for the two examples are

$$(i) \quad H_0 = \frac{p^2}{2} + \frac{Kx^2}{2} + \cos \theta \frac{b_2}{3!} x^3$$

$$(ii) \quad H_0 = \frac{p^2}{2} + \frac{Kx^2}{2} + \delta_p(\theta) \frac{b_3}{4!} x^4 .$$
(3.1)

Transforming to action-angle variables

$$(i) \quad H_0 = \frac{J_0}{\beta} + \cos \theta \frac{b_2 \sqrt{8}}{6} \beta^{\frac{3}{2}} J_0^{\frac{3}{2}} \cos^3 \phi_0$$

$$(ii) \quad H_0 = \frac{J_0}{\beta} + \delta_p(\theta) \frac{b_3}{6} J_0^2 \beta^2 \cos^4 \phi_0$$
(3.2)

where β is the beta function which, for the purpose of this model calculation we take to be

$$\beta = \frac{R}{\nu} = \frac{1}{\sqrt{K}} .$$
(3.3)

The radius of the ring has been set to unity so the independent variable is angular.

$G^{(1)}$ is calculated from Eq. (2.11)

$$(i) \quad G^{(1)} = -\frac{b_2 \sqrt{8}}{48} \beta^{\frac{3}{2}} J_1^{\frac{3}{2}} 2\text{Re}[e^{i3\phi_0} I_3(3, \theta_f) + 3e^{i\phi_0} I_3(1, \theta_f)]$$

$$(ii) \quad G^{(1)} = -\frac{b_3}{96} \beta^2 J_1^2 2\text{Re}[e^{i4\phi_0} e^{i4\nu(\theta_s - \theta_f)} + 4e^{i2\phi_0} e^{i2\nu(\theta_s - \theta_f)} + 3]$$
(3.4)

where θ_δ is the location of the delta octupole and I_3 is the integral:

$$\begin{aligned}
 I_3(k, \theta_f) &= \int_{\theta_i}^{\theta_f} \cos(\theta') e^{ik\nu(\theta' - \theta_f)} d\theta' \\
 &= \frac{-\frac{i}{2} e^{-ik\nu\theta_f}}{k^2\nu^2 - 1} [e^{ik\nu\theta'} (k\nu \cos \theta' - \sin \theta')]_{\theta_i}^{\theta_f}.
 \end{aligned} \tag{3.5}$$

Now we can use Eqs. (2.14) and (2.15) to find V_1 and $G^{(2)}$. Since the calculation of V_1 involves evaluating more than two hundred terms, we used the symbolic manipulation program REDUCE¹⁰ version 3.1 for many of the algebraic manipulations. A REDUCE program was written which, given an initial perturbation, would calculate $G^{(1)}$, V_1 , and $G^{(2)}$, and then write the results in the form of Fortran subroutines. The goal was to avoid the necessity of copying the expressions by hand where mistakes would likely have been made.

At this point it is useful to introduce a simple generalized method of writing $G^{(2)}$ which can be used to represent different perturbations. The obvious solution is to express it in terms of a power series in $J_2^{1/2}$ and a Fourier series in ϕ_1 ,

$$G^{(2)} = \sum_{k \geq 0, m} J_2^{\frac{m}{2}} 2\text{Re}[C_{km}(\theta) e^{ik\phi_1}]. \tag{3.6}$$

The range of k and m in the summation can be found by looking at the expression for V_1 , Eq. (2.14). For sextupoles or higher order perturbations the ranges are:

$$\begin{aligned}
 k_{max} &= 3p, & k_{min} &= 0 \\
 m_{max} &= (3p - 4), & m_{min} &= (2p - 2),
 \end{aligned} \tag{3.7}$$

where p is the order of the perturbation. Since the generating functions are invariant in θ once the steps $\Delta\theta$ are fixed, the $C_{km}(\theta)$ coefficients only need to be

calculated once. Thus calculating $G^{(2)}$ for a step on any turn is simply a matter of summing the series in ϕ_1 and J_2 . Actually, when tracking, we need the partial derivatives of $G^{(2)}$ with respect to ϕ_1 and J_2 , not $G^{(2)}$ itself, but in this series representation the calculation of the derivatives becomes trivial.

The particle's position in phase space is calculated at the end of each step from the position at the end of the previous step. When tracking to second order, this requires solving the implicit equations for ϕ and the explicit equations for J twice for each step. We use a simple Newton's iteration method to solve the implicit equations:

$$x_n = x_{n-1} - \frac{f(x_{n-1})}{f'(x_{n-1})}. \quad (3.8)$$

Since the perturbation is a small effect, ϕ_2 is a good approximation to ϕ_1 (as is ϕ_1 for ϕ_0) and can be used as a starting point for the Newton's method. In such a situation Newton's method converges quadratically to the solution, and despite the extra function evaluation, it is faster than simple iteration. Typically, a solution accurate to the computer's double precision arithmetic is found in three to four iterations.

In Figures 1 and 2 we show the results of tracking the two perturbations. Both plots are of $\sqrt{2J_0/\beta} \cos \phi_0$ vs. $-\sqrt{2J_0/\beta} \sin \phi_0$. The six initial conditions used to generate the curves are listed next to each plot. To heighten the effects of the perturbations the tune ν was set fairly close to $\frac{1}{3}$ for the case of the sextupole perturbation and $\frac{1}{4}$ for the case of the octupole. In both cases superconvergent tracking closely approximates the true motion.

The effects of the continuous sextupole perturbation can be calculated from Hamilton's equations using a differential equation solver. Figure 3 is a plot

Parameters: $b_3 = 0.01$
 $\beta = 2.90$

Initial Conditions

ϕ	J
1.0	0.05
1.0	0.20
1.0	0.50
1.0	1.20
1.0	1.80
1.27	14.40

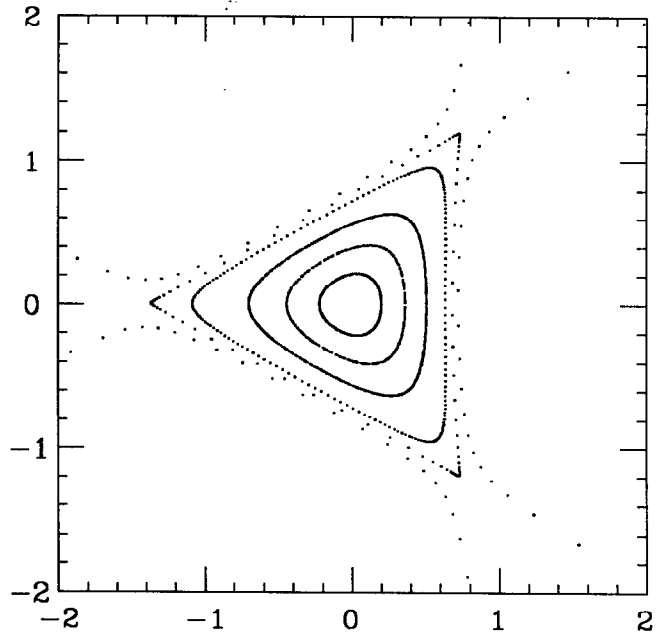


Fig. 1. Superconvergent tracking of the $\cos(\theta)x^3$ perturbation.

Parameters: $b_4 = 0.01$
 $\beta = 4.10$

Initial Conditions

ϕ	J
0.63	0.05
0.63	0.20
0.63	0.40
0.63	0.51
0.63	0.53
0.63	0.556

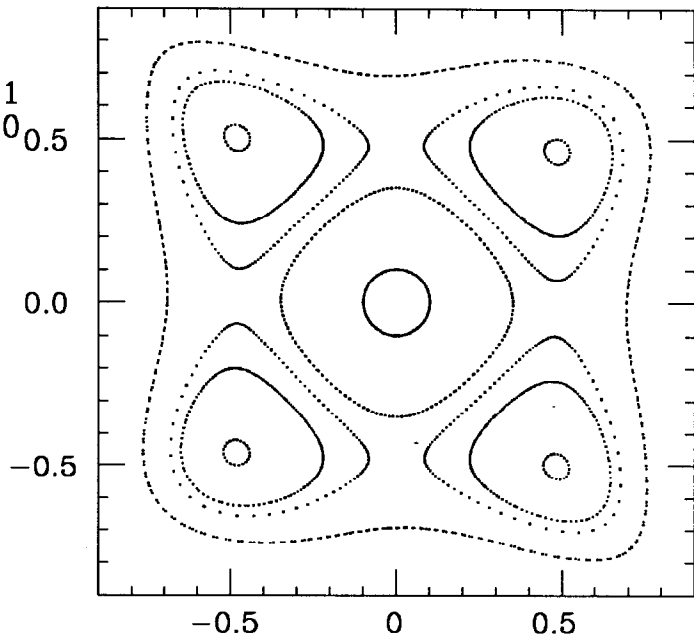


Fig. 2. Superconvergent tracking of the $\delta_p(\theta)x^4$ perturbation.

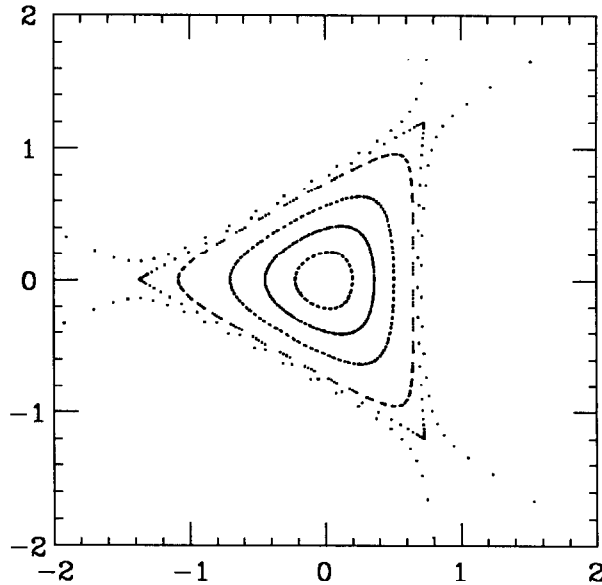


Fig. 3. Tracking of the $\cos(\theta)x^3$ perturbation by integrating Hamilton's differential equations.

generated in such a manner with the same parameter values and initial conditions as Figure 1. The only noticeable differences appear on the separatrices. The superconvergent tracking method is roughly eight times faster than EPSODE,¹¹ a routine which we use to integrate Hamilton's differential equations through the non-linear elements. Since the routines for tracking were written to test the method and not for speed, the results are encouraging.

For the case of a delta function perturbation, the true motion can be easily found by integrating the equations of motion. Hamilton's equations for the octupole perturbation are

$$\begin{aligned} \dot{x} &= p \\ \dot{p} &= -Kx - \delta(\theta) \frac{b_3}{6} x^3. \end{aligned} \tag{3.9}$$

The solution to these equations is a simple harmonic oscillation, except at the

location of the perturbation, θ_δ . At θ_δ , the momentum simply changes by $\frac{b_3}{6}x^3$. Thus to calculate the position at the end of one turn, we have the two maps

$$\begin{aligned}x_{\theta_\delta} &= x_i \cos(\nu\theta_\delta) + \frac{p_i}{\nu} \sin(\nu\theta_\delta) \\p_{\theta_\delta} &= -x_i\nu \sin(\nu\theta_\delta) + p_i \cos(\nu\theta_\delta) - \frac{b_3}{6}x_{\theta_\delta}^3\end{aligned}\tag{3.10}$$

and

$$\begin{aligned}x_{2\pi} &= x_{\theta_\delta} \cos(\nu(2\pi - \theta_\delta)) + \frac{p_{\theta_\delta}}{\nu} \sin(\nu(2\pi - \theta_\delta)) \\p_{2\pi} &= -x_{\theta_\delta}\nu \sin(\nu(2\pi - \theta_\delta)) + p_{\theta_\delta} \cos(\nu(2\pi - \theta_\delta)) .\end{aligned}\tag{3.11}$$

This ‘kick’ method is frequently used in accelerator design programs to track the effects of sextupole magnets by approximating them as delta functions. It is quite useful for element by element tracking, but cannot handle very long sextupole fields (such as errors in bending magnets) unless the magnets are subdivided and replaced with many kicks.

To verify that the errors in the second order superconvergent tracking are of order ϵ^4 , we tracked the sextupole perturbation with different values of b_2 , the perturbation strength. We set the β parameter to 2.90 and used $J_i = 1.20$ and $\phi_i = 1.0$ as the initial conditions. Figure 4 contains a plot of the absolute error of J_0 and ϕ_0 versus b_2 . The absolute error was found by subtracting the value of J or ϕ on tenth turn calculated with the superconvergent method from the J or ϕ value calculated with EPSODE, the differential equation solver. The other graph in Figure 4 is a plot of the logarithm of the same points. The slope of these lines show the power dependence of the error on b_2 . The slopes of the $\log(J_{err})$ versus $\log(b_2)$ line and $\log(\phi_{err})$ versus $\log(b_2)$ line are almost exactly 4.0 as they should be.

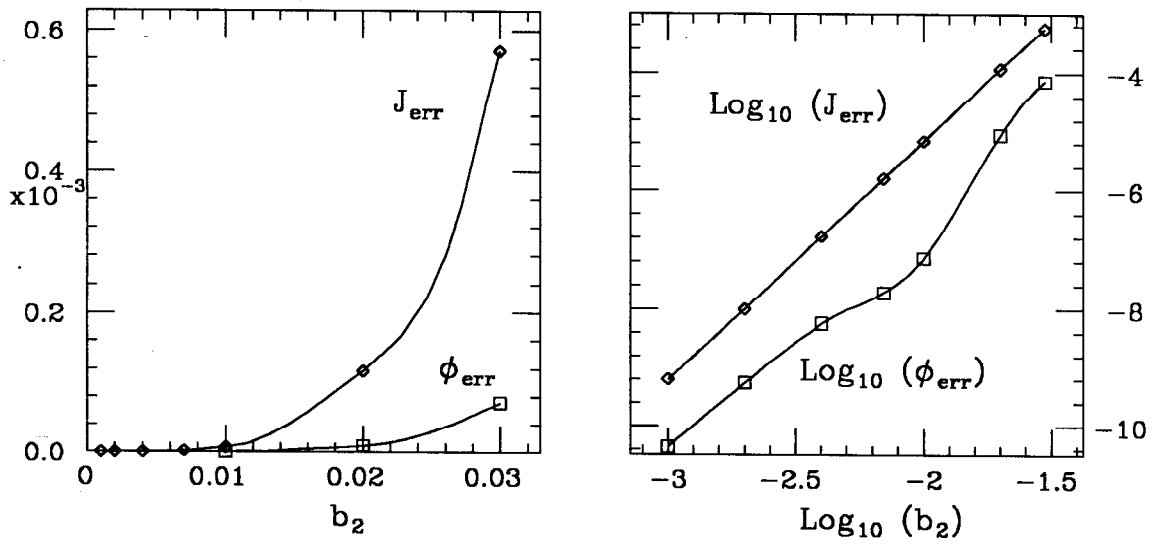


Fig. 4. Absolute error in J and ϕ vs. perturbation strength, b_2 .

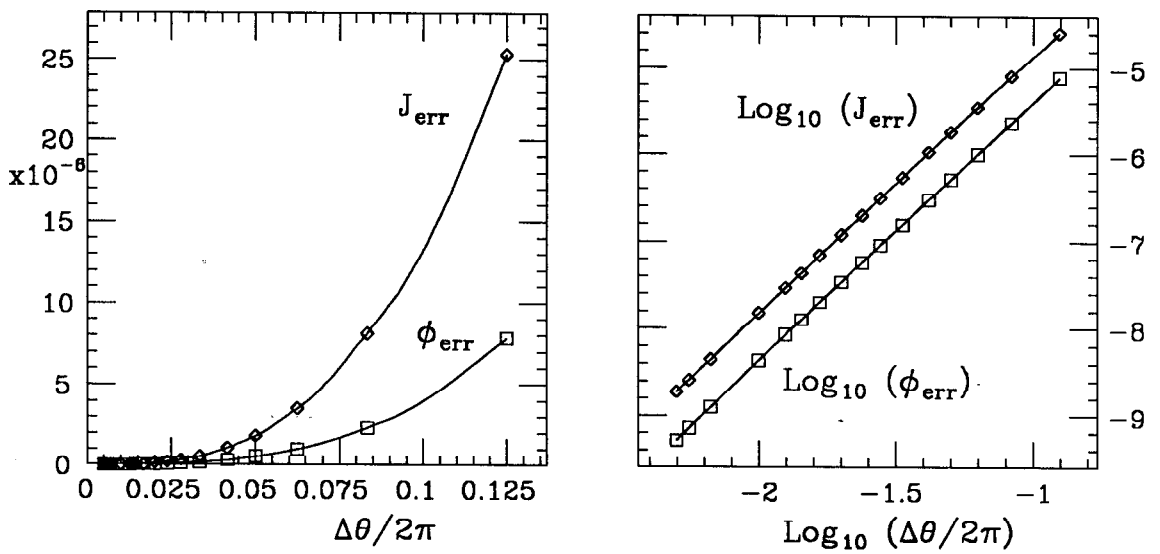


Fig. 5. Absolute error in J and ϕ vs. $\Delta\theta$.

Another diagnostic which we performed is to look at the small $\Delta\theta$ behavior. For small $\Delta\theta$, the $e^{im\nu(\theta' - \theta_f)}$ terms in the integral for $G^{(1)}$, Eq. (2.11), can be expanded. The result is that the lowest order of $\Delta\theta$ in $G^{(1)}$ are linear terms. The same is true in V_1 , as can be seen from Eq. (2.14). $G^{(2)}$ will have a $\Delta\theta^2$ dependence, for small $\Delta\theta$, and thus the lowest order of $\Delta\theta$ in H_2 will be cubic (see Eqs. (2.19) and (2.20)). The cubic dependence is displayed in Figure 5, where we plot the absolute error in J and ϕ versus $\Delta\theta/2\pi$ for the case of the sextupole perturbation. We also plot the logarithm of the points, and one can see that the error is of order $(\Delta\theta/2\pi)^3$.

4. TWO DEGREES OF FREEDOM

In this section we move to two degrees of freedom and to the problem of motion in an 'arbitrary' accelerator lattice. The Hamiltonian for oscillation about the closed orbit in a circular accelerator with an arbitrary sextupole field is

$$H_0 = \frac{p_x^2}{2} + \frac{p_y^2}{2} + \frac{K_x(s)x^2}{2} + \frac{K_y(s)y^2}{2} + \frac{b_2(s)}{3!}(x^3 - 3xy^2), \quad (4.1)$$

where $K(s)$ is the focusing function and $b_2(s)$ is the sextupole strength:

$$b_2(s) \equiv \frac{e}{p_0 c} \left. \frac{\partial^2 B_y}{\partial x^2} \right|_{\substack{y=0 \\ x=0}}.$$

In action-angle variables this becomes

$$H_0 = \frac{J_x}{\beta_x(s)} + \frac{J_y}{\beta_y(s)} + \frac{b_2(s)\sqrt{8}}{6} [\beta_x^{\frac{3}{2}}(s) J_x^{\frac{3}{2}} \cos^3 \phi_x - 3\beta_x^{\frac{1}{2}}(s)\beta_y(s) J_x^{\frac{1}{2}} J_y \cos \phi_x \cos^2 \phi_y] \quad (4.2)$$

where $\beta_x(\beta_y)$ is the beta function in the x (y) direction. Note that we assume the bending magnets and quadrupoles are separate and did not include those cross terms. Also, we are now using s , the distance around the ring, instead of θ as the independent variable.

The first order generating function used for tracking, $G^{(1)}(\phi_0, \mathbf{J}_1, s)$, is calculated from Eq. (2.11)

$$G^{(1)} = -\frac{\sqrt{8}}{48} J_x^{\frac{3}{2}} [e^{3i\phi_x} I_{31}(3, 3, 0) + 3e^{i\phi_x} I_{31}(3, 1, 0) + \text{CC}] + \frac{\sqrt{8}}{16} J_x^{\frac{1}{2}} J_y [e^{i(\phi_x + 2\phi_y)} I_{31}(1, 1, 2) + 2e^{i\phi_x} I_{31}(1, 1, 0) + e^{i(\phi_x - 2\phi_y)} I_{31}(1, 1, -2) + \text{CC}], \quad (4.3)$$

where "CC" represents the complex conjugate. I_{31} is defined as the integral:

$$I_{31}(n, \mathbf{m}, s_f) = \int_{s_i}^{s_f} b_2 \beta_x^{\frac{n}{2}} \beta_y^{\frac{3-n}{2}} e^{im \cdot [\psi(s') - \psi(s_f)]} ds' , \quad (4.4)$$

where b_2 , β_x , and β_y are all periodic functions of s' . Since the phase advance is no longer uniform, the solution is in terms of $\psi(s)$ instead of $\nu\theta$, where

$$\psi_i(s) \equiv \int_0^s \frac{ds'}{\beta_i(s')} . \quad (4.5)$$

It is obvious that the integrals, I_{31} , are invariant if both s_f and s_i are shifted by one period of the structure, and therefore they do not have to be re-calculated for each iteration of the ring.

To now calculate the second order generating function we need to calculate $H_1(\phi_1, \mathbf{J}_1, \theta)$ from $G^{(1)}$ and V_0 . H_1 , in two degrees of freedom, is calculated in an analogous manner to that in one degree of freedom (see Eq. (2.13)),

$$H_1 = \frac{J_{1x}}{\beta_x(s)} + \frac{J_{1y}}{\beta_y(s)} + V_1(\phi_1, \mathbf{J}_1, \theta) \quad (4.6)$$

and

$$\begin{aligned} V_1 = & V_{J_x} G_{\phi_x} + \frac{1}{2} V_{J_x J_x} G_{\phi_x}^2 - V_{J_x \phi_x} G_{J_x} G_{\phi_x} - V_{J_x} G_{J_x} G_{\phi_x \phi_x} \\ & + V_{J_y} G_{\phi_y} + \frac{1}{2} V_{J_y J_y} G_{\phi_y}^2 - V_{J_y \phi_y} G_{J_y} G_{\phi_y} - V_{J_y} G_{J_y} G_{\phi_y \phi_y} \\ & + V_{J_x J_y} G_{\phi_x} G_{\phi_y} - V_{J_y \phi_x} G_{\phi_y} G_{J_x} - V_{J_y} G_{J_x} G_{\phi_x \phi_y} \\ & - V_{J_x \phi_y} G_{\phi_x} G_{J_y} - V_{J_x} G_{J_y} G_{\phi_x \phi_y} , \end{aligned} \quad (4.7)$$

where G is $G^{(1)}$ and V is V_0 . For the case of an arbitrary sextupole distribution, $G^{(1)}$ and H_0 are calculated in Eqs. (4.3) and (4.2) respectively. Now $G^{(2)}$ is

calculated by integrating V_1 , as in Eq. (2.15). The calculation of $G^{(2)}$ for the 2-D case involves the evaluation of over four thousand terms. Very roughly there should be 2^4 times the number of terms in the 1-D case since there are over twice as many terms in V_0 , $G^{(1)}$, and V_1 . Again, we used the algebraic manipulation program, REDUCE version 3.1, to perform the calculation, and again we express $G^{(2)}$ as a power series in J_2 and a Fourier series in ϕ_1

$$G^{(2)} = \sum_{m,n,k \geq 0, l} J_{2x}^{\frac{m}{2}} J_{2y}^{\frac{n}{2}} 2\text{Re}[C_{mnkl}(s)e^{ik\phi_{1x}}e^{il\phi_{1y}}] \quad (4.8)$$

where the summation limits can be calculated in an analogous manner as Eqs. (3.7). For the case of the sextupole perturbation:

$$\begin{aligned} -1 \leq m \leq 5 & & 0 \leq n \leq 6 \\ 0 \leq k \leq 9 & & -6 \leq l \leq 6. \end{aligned} \quad (4.9)$$

If we were to sum over the full range of each index there would be over 6,000 terms in the sum, but there are only 87 non-zero coefficients, C_{mnkl} (these are tabulated in Appendix A). Thus we use a number of simple rules which can be derived from the expressions for $G^{(1)}$ and V_0 and from the form of V_1 :

- 1) $n = 2 \lfloor \frac{5-m}{2} \rfloor$.
- 2) $l = 0$ if $n = 0$.
- 3) l is always even.
- 4) $\begin{cases} k \text{ is always even,} & \text{if } m \text{ is even;} \\ k \text{ is always odd,} & \text{if } m \text{ is odd.} \end{cases}$
- 5) $\begin{cases} k \leq m + 2, & \text{if } m \text{ is even;} \\ k \leq m + 4, & \text{if } m \text{ is odd.} \end{cases}$
- 6) $\begin{cases} |l| \leq 4, & \text{if } m \text{ is even;} \\ |l| \leq 6, & \text{if } m \text{ is odd.} \end{cases}$

These rules, which can be implemented quickly and easily, reduce the sum to 97 terms of which only 10 are zero and therefore unnecessary.

As in the case of $G^{(1)}$, the coefficients of the series for $G^{(2)}$, the C_{mnl} 's, need only be calculated once for each step. Since V_1 contains multiplicative combinations of the I_{31} type integrals in Eq. (4.4), the coefficients contain double integrals of the forms:

$$I_{32}(n, \mathbf{m}, \mathbf{p}', s_f) = \int_{s_i}^{s_f} b_2 \beta_x^{\frac{n}{2}} \beta_y^{\frac{3-n}{2}} e^{i\mathbf{m} \cdot [\boldsymbol{\psi}(s) - \boldsymbol{\psi}(s_f)]} I_{31}(\mathbf{p}', s) ds \quad (4.10)$$

and

$$I_{33}(n, \mathbf{m}, \mathbf{p}', \mathbf{p}'', s_f) = \int_{s_i}^{s_f} b_2 \beta_x^{\frac{n}{2}} \beta_y^{\frac{3-n}{2}} e^{i\mathbf{m} \cdot [\boldsymbol{\psi}(s) - \boldsymbol{\psi}(s_f)]} \times \quad (4.11)$$

$$I_{31}(\mathbf{p}', s) I_{31}(\mathbf{p}'', s) ds ,$$

where \mathbf{p}' and \mathbf{p}'' are the parameters (n', \mathbf{m}') and (n'', \mathbf{m}'') respectively. The number of these integrals needed was reduced by using simple rules derived from integrating by parts. In final form the expressions for the coefficients require the ten possible I_{31} integrals, fifty-four I_{32} integrals, and one hundred and seventy-five I_{33} integrals.

In the 1-D cases we used REDUCE to perform the integrations analytically since the θ dependence of b_2 , b_3 and β was explicitly specified. When tracking actual rings, it is more convenient to calculate the integrals numerically. In this case one can specify the ring with an accelerator lattice program such as MAD¹² or COMFORT¹³ and use the calculated β 's etc. to evaluate the integrals. A detailed description of the methods we use is given in Appendix C.

It is worth noting at this point that these integrals can provide useful information when designing a lattice. All first order geometric aberrations due to the sextupoles will disappear when the I_{31} integrals are all zero. Likewise all aberrations up to fourth order in the sextupole strength will disappear when the I_{32} and I_{33} integrals are all zero. The I_{31} integrals will be largest when the phase advance between sextupoles, $\delta\Psi$, is of the form:

$$\begin{aligned} \delta\Psi_x &= 2n\pi, & 3\delta\Psi_x &= 2n\pi \\ \delta\Psi_x \pm 2\delta\Psi_y &= 2n\pi. \end{aligned} \tag{4.12}$$

These are just the sextupole resonances. The I_{31} integrals can be minimized by adjusting the sextupole strengths and their locations. For example, to zero the I_{31} integrals over N identical cells ($N > 3$), one can choose the phase advance per cell, Ψ , such that

$$\begin{aligned} \Psi_x &= 2n_1\pi/N \\ \Psi_x + 2\Psi_y &= 2n_2\pi/N & \Psi_x - 2\Psi_y &= 2n_3\pi/N \end{aligned} \tag{4.13}$$

where n_1 , n_2 , and n_3 are all integers. In this case the integrals can be written:

$$I_{31} = e^{-i\mathbf{m}\cdot\boldsymbol{\psi}(s_f)} \left[\int_{\text{first cell}} b_2(s)\beta_x\beta_y e^{i\mathbf{m}\cdot\boldsymbol{\psi}(s)} ds \right] \sum_{n=0}^{N-1} e^{i(\mathbf{m}\cdot\Psi)n}. \tag{4.14}$$

The integrals will be zero since the summation of the complex exponential is equal to zero.

When using the superconvergent tracking algorithm, the ring is divided into steps $\theta_i \rightarrow \theta_f$ over which the integrals are calculated. The variables \mathbf{J} and ϕ are then evaluated at the end of each step. Since the sextupole strength is a discontinuous function of the azimuth around the ring, the errors do not obey

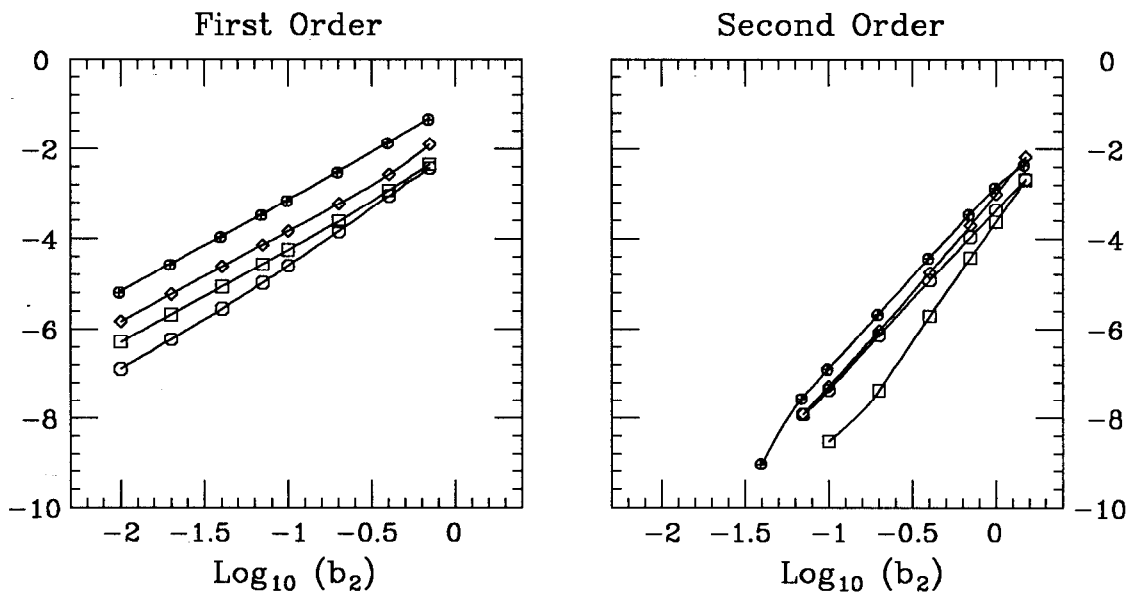


Fig. 6. Log plots of errors *vs.* perturbation strength, b_2 , for 1st and 2nd order tracking.

the power laws of Eq. (2.19) and Eq. (2.20). The accuracy of the algorithm is then a complicated function of the steps chosen. In general one increases the accuracy by increasing the number of steps, but we cannot offer any rigorous rules for choosing the steps; we simply compared the error for various step sizes and then chose one so that it was not possible to visually discern the difference between the superconvergent tracking and the 'exact' solutions from EPSODE. A procedure to estimate the error of the various step sizes is presented later in this section.

As in the 1-D cases, the performance of the superconvergent tracking algorithm was verified by comparing the errors versus the sextupole strength, b_2 . Figure 6 contains plots of errors for both first and second order calculations. As before the absolute values were calculated with EPSODE. We compare the two

tracking methods after calculating twenty points in a test lattice with a single sextupole whose strength was varied. The logarithms of the absolute errors for ϕ_x and ϕ_y are plotted as \square and \circ and the logarithms of the relative errors for J_x and J_y are plotted as \diamond and \oplus respectively. We chose to plot the relative errors for J_x and J_y to keep the ϕ errors and the J errors on the same scale; the J values were of order 10^{-7} while the ϕ values were of order unity. The scales of the two plots in Figure 6 are the same, displaying the difference in the slopes of the first and second order calculations and the dependence of the errors on b_2 . As described in Section 2, the errors in first order tracking should be proportional to $(b_2)^2$, while those for the second order should go as $(b_2)^4$. It is evident from Figure 6 that both calculations perform as they should.

In testing the 1-D cases, the dependence of the errors on $\Delta\theta$, the step size, was also checked. It was not possible to do this for our 2-D program because each magnet is treated as a unit which can be concatenated with others, but not subdivided. Since, in general, adjacent sextupoles have neither the same strength nor the same values of β_x or β_y , the integrals forming $G^{(1)}$, Eq. (2.11), are not linear functions of $\Delta\theta$. The errors decrease with $\Delta\theta$, but the values oscillate within a decreasing envelope and thus we were not able to explicitly show the power law dependence.

The fact that the errors do not obey a power law dependence on $\Delta\theta$ makes it more difficult to estimate the error on any given turn. For most typical sextupole configurations the error when tracking with one step per magnet is very close to the computer accuracy and thus can be used as an exact solution. A more accurate result can be obtained using the power law dependence on $\Delta\theta$ if all of the magnets in the lattice with a sextupole field are divided in half so there are

	Est. Diff.	True Diff.	Rel. Error
ϕ_x	0.254×10^{-3}	0.266×10^{-3}	6.05×10^{-6}
J_x	-0.858×10^{-10}	-0.951×10^{-10}	7.47×10^{-6}
ϕ_y	-0.371×10^{-4}	-0.364×10^{-4}	3.59×10^{-7}
J_y	-0.147×10^{-9}	-0.163×10^{-9}	7.79×10^{-6}

Table 1. Error estimates of 2nd order tracking

two identical adjacent magnets. Now if one compares the results of tracking with steps of half a magnet to that with steps of the full magnets, one can get an accurate estimate of the error using Eq. (2.21):

$$(f_1 - f_{true}) = \alpha = \frac{f_1 - f_{1/2}}{(1 - 1/8)}, \quad (4.15)$$

where f_1 and $f_{1/2}$ are the values of $J_{x,y}$ or $\phi_{x,y}$ for steps of a full magnet and a half magnet respectively.

We used this procedure to estimate the errors of tracking 200 turns of the *SSCerr* lattice, described in the next section and listed in Appendix B. The results are listed in Table 1. The ‘Est. Diff.’ column, calculated using Eq. (4.15), lists the estimated difference between the exact values and results of tracking with one step per magnet, and the ‘True Diff.’ values were found by comparing tracking with results from EPSODE. The relative error is the error between the value found by adding the estimated difference to the tracking result and the value from EPSODE. The difference between the actual error and our estimates was less than 10% in each case, and as can be seen, the solution found by adding the estimated difference to the tracking data is very close to the exact solution.

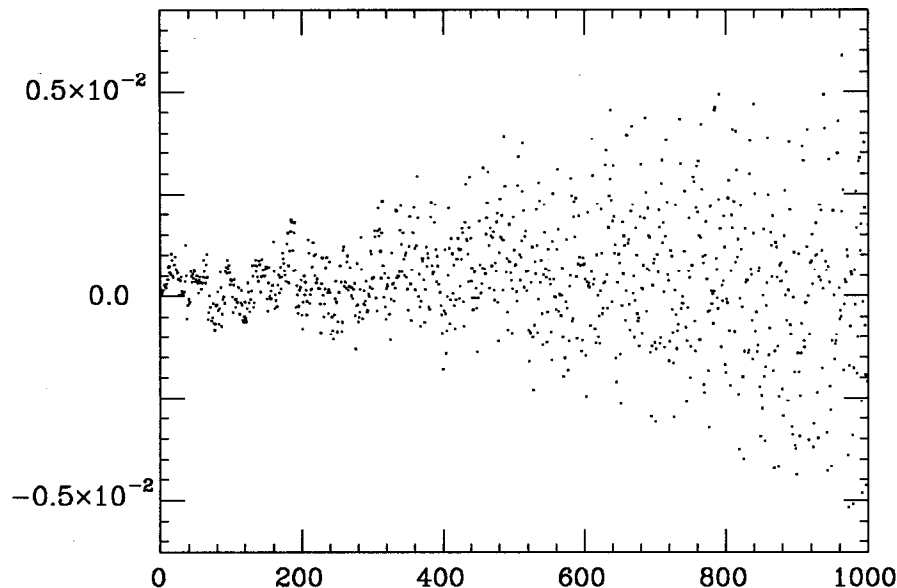


Fig. 7. Relative error vs. turn number in 2nd order tracking of *SSCerr*.

The disadvantage of this method is that it is slow. To arrive at the estimate we had to track the lattice with 56 steps and with 112 steps per turn when we usually use 4. Such error estimates are useful to see how accurate a choice of step size is over a small number of turns and then extrapolate the error to a larger number of steps. The extrapolation is difficult since the error does not depend linearly on the number of turns. However, on the cases we tested, the *envelope* of the error is approximately a linear function of the number of turns and can be estimated from the envelope of the first 200 turns. Figure 7 is a plot of the relative error of J_x for the *SSCerr* lattice with initial conditions $(J_x, J_y) = (4. \times 10^{-7}, 4. \times 10^{-7})$ and $(\phi_x, \phi_y) = (0.0, 0.0)$ with 4 steps per turn. The error of J_x was larger than that of J_y , ϕ_x , and ϕ_y in this case.

In Figure 8 we compare the results of second order tracking with the dif-

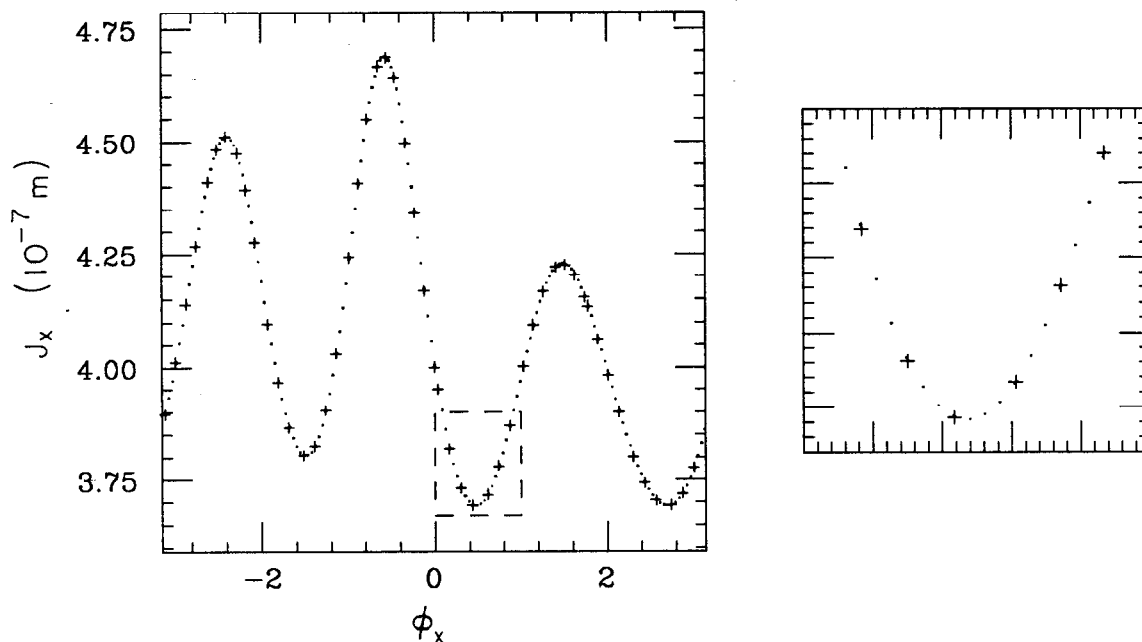


Fig. 8. 2nd order tracking of *SSCerr* compared to tracking by EPSODE.

ferential equation solver, EPSODE. The lattice used was *SSCerr* which is described in the next section and listed in Appendix B. With initial conditions of $(J_x, J_y) = (4.0 \times 10^{-7}, 0.0)$ and $(\phi_x, \phi_y) = (0.0, 0.0)$, the distortion in J_x was about 20% of the mean amplitude. Note that since $J_y = 0.0$, this has one degree of freedom only, and the plots are of J_x vs. ϕ_x . The results from the superconvergent tracking are plotted as dots and the results from EPSODE are plotted as crosses. The plot on the right is a blow-up of the box outlined in the left-hand plot; obviously the difference between the two is very small. We used four steps per turn of the lattice, and the non-optimized superconvergent tracking program ran roughly 30 times faster than EPSODE.

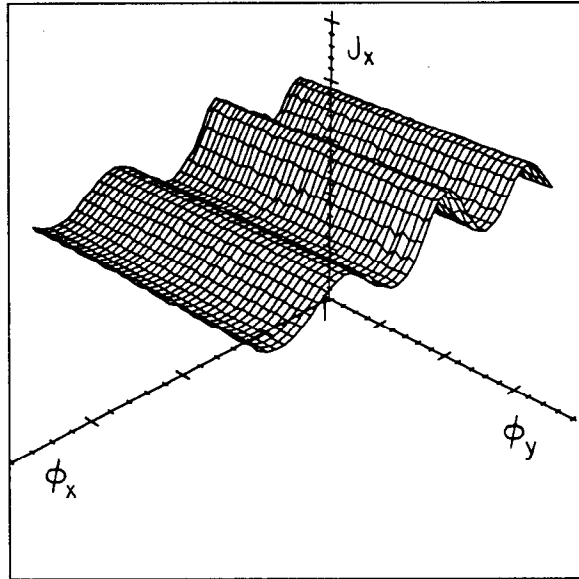


Fig. 9. 2nd order tracking of *SSCerr*: $J_x = 4. \times 10^{-7}$, $J_y = 0.0$,
 $\phi_x = \phi_y = 0.0$ and the tunes are: $\nu_x = 2.265$, $\nu_y = 2.285$.

5. TRACKING THE SSC¹⁴

In this section we use the 2-D program to track a section of the SSC (Superconducting Super Collider) arcs. We take fourteen arc cells of the form: QD, SD, BEND, QF, SF, BEND, where the symbol QD represents a defocusing quadrupole magnet, SD is a defocusing sextupole, QF is a focusing quadrupole, SF is a focusing sextupole, and BEND represents five sequential bending magnets which we concatenated into one bend with the same total length and bending angle. The accelerator design program MAD was then used to adjust the quadrupole strengths to fit the appropriate fractional SSC tunes, $\nu_x = .265$ and $\nu_y = .285$. The phase advance per cell for the SSC is specified to be sixty degrees, thus we use $\nu_x = 2.265$ and $\nu_y = 2.285$ for the 14 cells. The MAD input deck of our lattice, called *SSC*, is listed in Appendix B. Starting with the nominal lattice

we add random sextupole error fields to the bend magnets where the RMS field strength was chosen to be the order of the specification in the SSC design handbook: $K2_{rms} = 1.9786 \times 10^{-4} \text{m}^{-3}$. Note the units here are the units used in MAD not the units of the SSC specifications. The set of random fields used had $K2_{rms} = 1.873 \times 10^{-4} \text{m}^{-3}$ and $K2_{ave} = 2.520 \times 10^{-5} \text{m}^{-3}$. This lattice is called *SSCerr* and is also listed in Appendix B.

Figure 9 is a plot of J_x versus ϕ_x and ϕ_y generated with the second order superconvergent tracking program. The initial values are $(J_x, J_y) = (4. \times 10^{-7}, 0.0)$ and $(\phi_x, \phi_y) = (0.0, 0.0)$. The initial value of J_x corresponds to a displacement of $\Delta x \approx 1.6 \text{ cm}$, calculated using $\beta = 333 \text{ m}$. Note that the initial values are the same as in Figure 8, but in Figure 8 J_x was plotted against ϕ_x while here we plot J_x versus ϕ_x and ϕ_y .

The meshes are created by ruling the two-dimensional surfaces on which the data points lie. Typically it takes about ten thousand points to sufficiently populate the entire 2-D surface so that a 40×40 mesh can be generated. The existence of the surface (a 2-torus) reflects the presence of the two invariants in a (nearly) integrable system and the fact that all of the data points evolve from the same initial state.⁸ In Figure 8 it is not necessary to display the data in this manner; however, in general the X and Y motions are coupled, making it very hard to interpret projections on the (J_x, ϕ_x) or (J_y, ϕ_y) planes. See Figures 11 and 12 for comparison. Figure 11 is a plot of two mesh surfaces (J_x, ϕ_x, ϕ_y) and (J_y, ϕ_x, ϕ_y) while Figure 12 contains the projections of the same data onto the (J_x, ϕ_x) and (J_y, ϕ_y) planes. Finally we note that in all of the mesh surface plots displayed, the scales are set such that the origin is at $J = \phi_x = \phi_y = 0.0$.

Figures 10 and 11 are plots of tracking *SSC* and *SSCerr* with the same initial

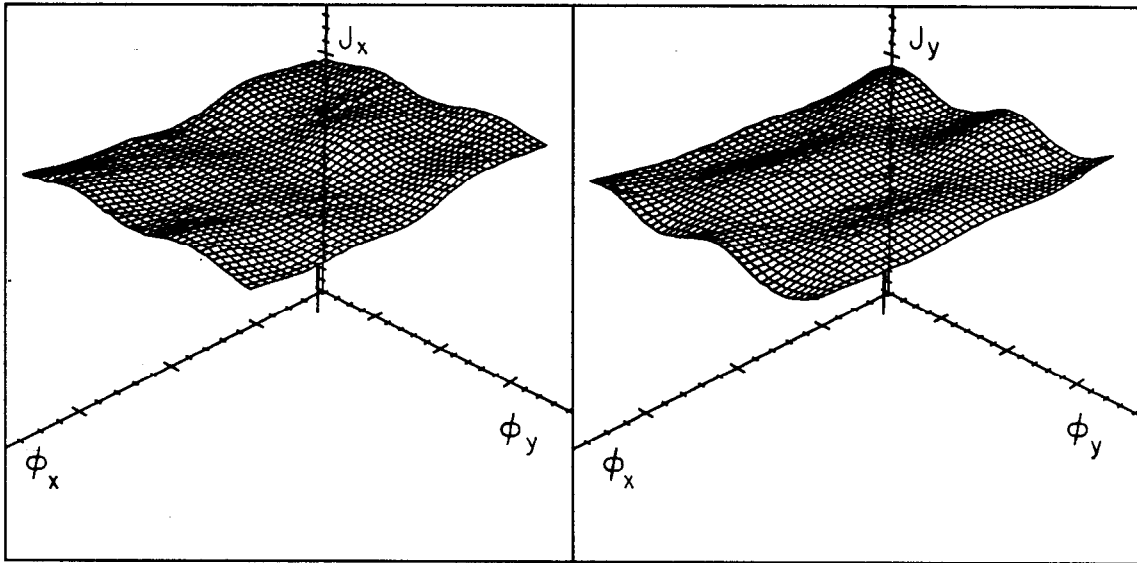


Fig. 10. 2nd order tracking of *SSC*: $J_x = 4. \times 10^{-7}, J_y = 4. \times 10^{-7}$.

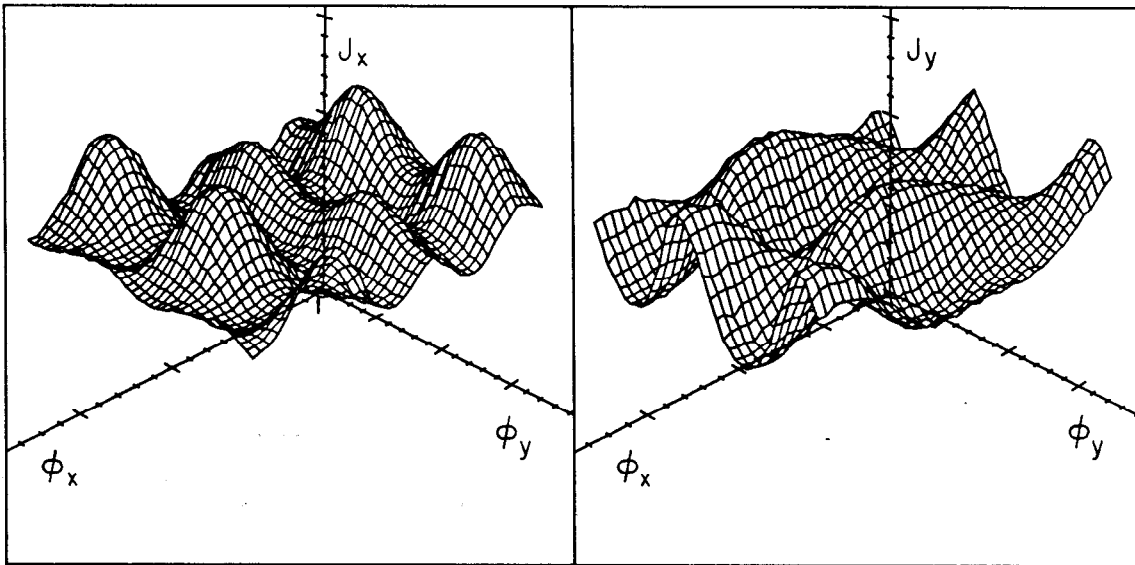


Fig. 11. 2nd order tracking of *SSCerr*: $J_x = 4. \times 10^{-7}, J_y = 4. \times 10^{-7}$.
The same initial conditions as Figure 10.

conditions: $(J_x, J_y) = (4. \times 10^{-7}, 4. \times 10^{-7})$ and $(\phi_x, \phi_y) = (0.0, 0.0)$. In both figures the left-hand plot is of J_x versus ϕ_x and ϕ_y , while the plot on the right is of J_y versus the two ϕ variables. The large distortions in Figure 11 are a result of the relatively small sextupole errors added to the bending magnets. Figure 10 was generated using 2 steps per turn of the ring while 4 steps were used in creating Figure 11, thus in both cases 14 sextupole field magnets were concatenated in each step. When calculating the data for Figure 10, the 2nd order superconvergent tracking took 0.023 sec./point on an IBM 370. This is roughly 30 times faster than EPSODE. In comparison, the data for Figure 11 was generated at a rate of 0.040 sec./point while EPSODE was more than 40 times slower. The decrease in speed of EPSODE when tracking the *SSCerr* lattice is a result of tracking through the sextupole fields in the bend magnets. Note that these times are given as reference points; the superconvergent tracking algorithm has not been optimized in ways other than described with regards to the summation of $G^{(2)}$, the second order generating function. For example, we use a simple iteration method to solve the implicit equations for ϕ which takes roughly 8 iterations for each order in each dimension. Obviously there are more efficient methods of solving these equations.

Figure 12 contains plots of tracking *SSCerr* with $(J_x, J_y) = (4. \times 10^{-7}, 4. \times 10^{-7})$ and $(\phi_x, \phi_y) = (0.0, 0.0)$, the same as Figure 11 except that the left plot is a projection of J_x onto the (J_x, ϕ_x) plane and right plot is the projection of J_y onto the (J_y, ϕ_y) plane. It is included to show the advantages of displaying data in the form of projected 2-D surfaces.

Finally, Figures 13 and 14 are invariant surfaces calculated with first order perturbation theory of the *SSC* and *SSCerr* lattices for the same initial conditions

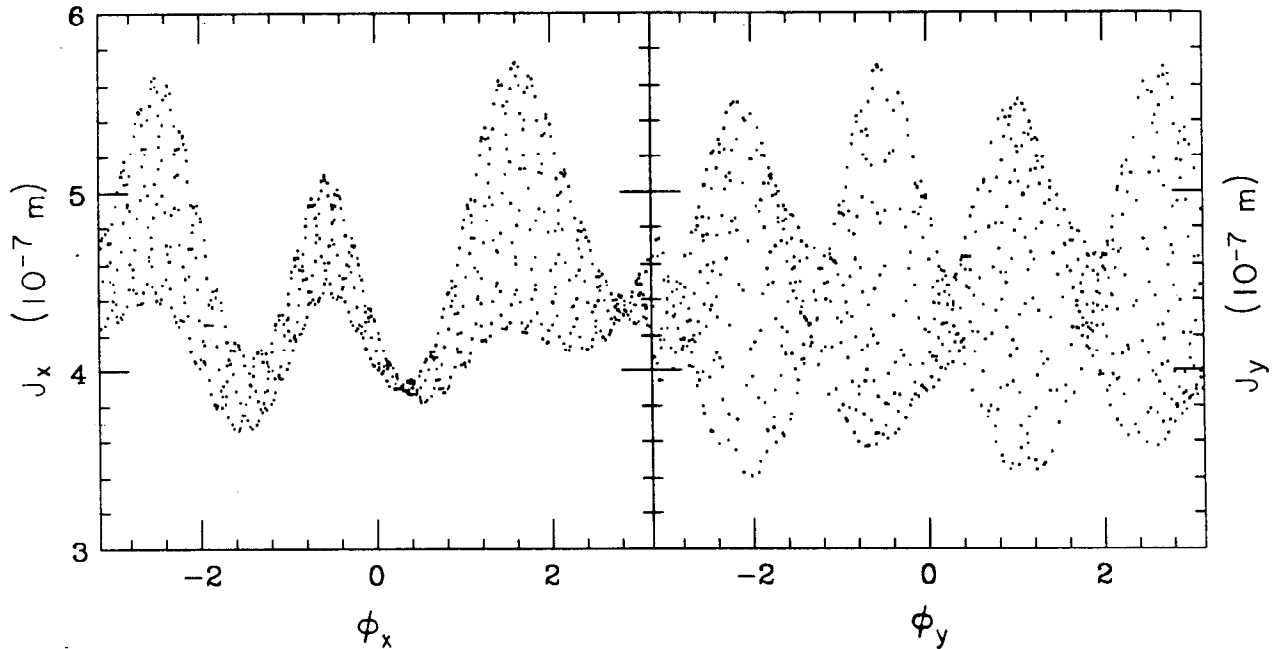


Fig. 12. 2nd order tracking of *SSCerr*: $J_x = 4. \times 10^{-7}$, $J_y = 4. \times 10^{-7}$.
The data plotted is the same as in Figure 11.

as Figures 10 and 11. The invariant surfaces from 1st order perturbation theory are calculated by the program since the necessary integrals can be found from the integrals calculated for the 1st order superconvergent tracking. Appendix D describes the details of the invariant surface calculations. Figure 15 is a comparison of the 1st order invariant surface calculation and the 2nd order superconvergent tracking with one degree of freedom. The dots are the tracking while the solid curve is the invariant surface. Obviously there is a large-discrepancy. The two techniques converge, as they should, as the sextupole strength is reduced.

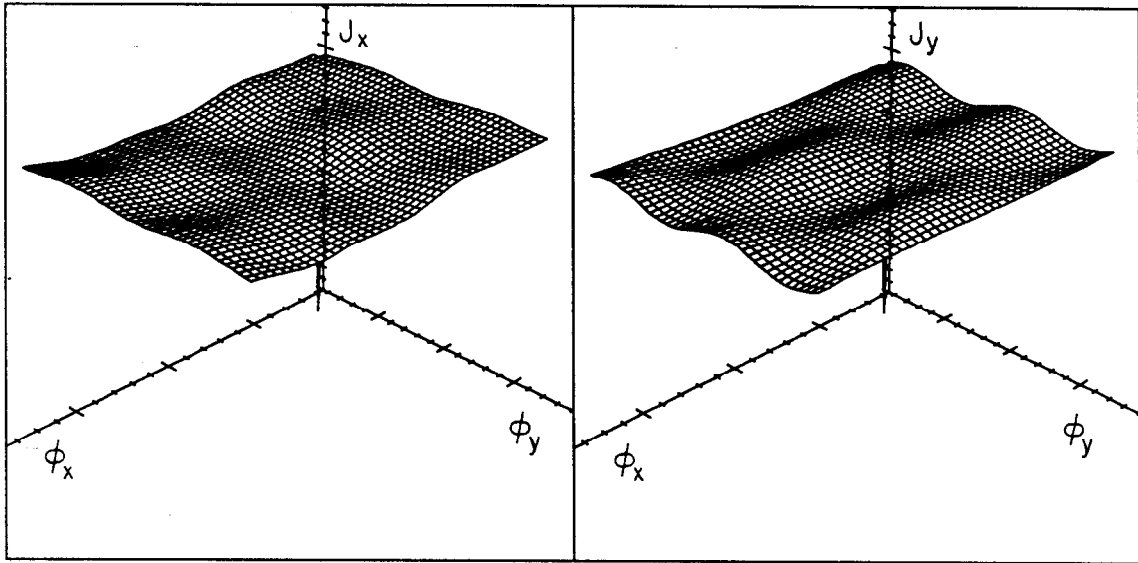


Fig. 13. Invariant surface of *SSC*: $J_x = 4. \times 10^{-7}, J_y = 4. \times 10^{-7}$.
Same initial conditions as Figures 10 and 11.

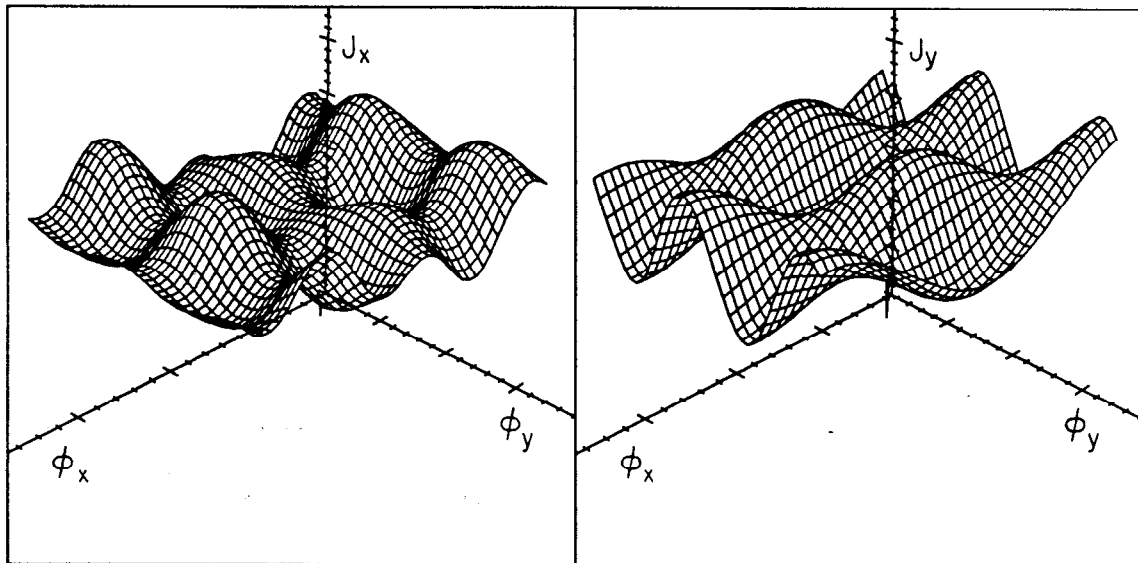


Fig. 14. Invariant surface of *SSCerr*: $J_x = 4. \times 10^{-7}, J_y = 4. \times 10^{-7}$.
Same initial conditions as Figures 10 and 11.

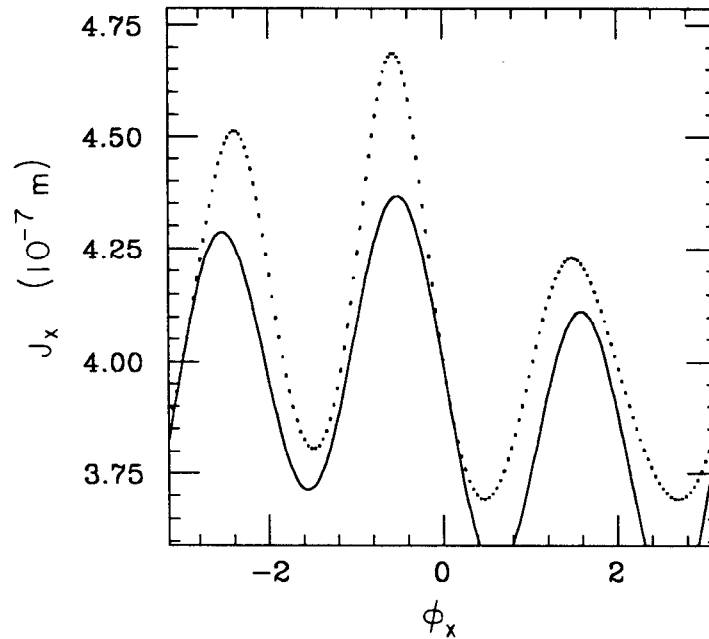


Fig. 15. Comparison of 2nd order tracking vs. 1st order invariant surface.

6. DISCUSSION

In this paper we have introduced a new tracking algorithm to track a particle through an accelerator lattice. Our method is closely tied to the analytic techniques used to calculate invariant surfaces. Some of the advantages of this algorithm over more conventional methods are that: (1) many elements can be concatenated and tracked in a single step, (2) long elements such as error fields in bending magnets are easily handled, (3) it is relatively fast, *i.e.* useful for the study of long term stability, and (4) the method is self checking in that one can test for convergence simply by reducing the step size.

We illustrated the technique with two test cases in one degree of freedom and then treated the case of two degrees of freedom when tracking an arbitrary

accelerator lattice with sextupoles. In both cases we used REDUCE to perform the analytic manipulations since the expressions become very complicated. This has the advantage of eliminating mistakes when transcribing the expressions to Fortran routines. After demonstrating that the algorithm performed correctly in both one and two degrees of freedom, it was used to track a segment of the SSC arcs as an example.

One of the problems with superconducting magnets is that it is harder to control the multipole error fields since the field shape is strongly determined by the conductor placement. Therefore, we compared the SSC with random field errors to the SSC without. We used two lattices of 14 arc cells, one with random sextupole errors in the bending magnets where the RMS field strength was taken from the SSC Parameter List,¹⁴ and one without bending magnet errors. It was found that while the sextupole magnets alone did not disturb the orbit much, the addition of the random errors to the bends caused some large distortions.

In studying the case of two degrees of freedom we found it quite useful to use a new technique of displaying the tracking data which was first introduced in Ref. 8. By displaying the data in perspective as shown in Figs. 9, 10, and 11, it is possible to untangle the invariant surfaces. In an integrable system the motion will always lie on a surface in these perspective plots. Large scale chaotic behavior can thus be viewed as departures from the surface. In the cases shown here the data was ruled to guide the eye; however, this is not essential.

Finally, we should explain what is meant by calling the algorithm *relatively* fast. We have not performed any serious timing tests against the standard tracking codes because we have not yet attempted to optimize the algorithm. In addition since this technique has wide applicability, speed is not always the key

issue. We have timed it against EPSODE and a kick code we wrote which treats sextupoles as delta functions. While the algorithm is much faster than EPSODE, it is slower than the kick code when tracking the *SSC* lattice. Of course, our kick code *cannot* be used to track through a lattice with finite length sextupole fields such as the *SSCerr* lattice without either subdividing the magnets or using a higher order symplectic integration technique.

To conclude, we have added yet another tool to the growing arsenal of tracking algorithms which are useful for understanding nonlinear effects in storage rings and transport lines. The ultimate utility of superconvergent tracking can be tested only by further detailed application to various problems in the tracking of particle beams.

APPENDIX A

A List of Non-Zero Elements in 2-D $G^{(2)}$ Summation

This is a listing of the non-zero $C_{mnl}(s)$ coefficients of the second order generating function, $G^{(2)}$, for the 2-D sextupole perturbation

$$G^{(2)} = \sum_{m,n,k \geq 0, l} J_x^{\frac{m}{2}} J_y^{\frac{n}{2}} 2\text{Re}[C_{mnl}(s)e^{ik\phi_x}e^{il\phi_y}] .$$

Listing of m , n , k , and l Subscripts for Non-zero C_{mnl} 's

<u>m</u>	<u>n</u>	<u>k</u>	<u>l</u>	<u>m</u>	<u>n</u>	<u>k</u>	<u>l</u>
-1	6	1	-6 - 6	-1	6	3	-6 - 6
0	4	0	-4 - 4	0	4	2	-4 - 4
1	4	1	-6 - 6	1	4	3	-6 - 6
1	4	5	-4 - 4	2	2	0	-4 - 4
2	2	2	-4 - 4	2	2	4	-2 - 2
3	2	1	-6 - 6	3	2	3	-6 - 6
3	2	5	-4 - 4	3	2	7	-2 - 2
4	0	0	0	4	0	2	0
4	0	4	0	5	0	1	0
5	0	3	0	5	0	5	0
5	0	7	0	5	0	9	0

where all l values in a range are even.

APPENDIX B

MAD Input Decks for *SSC* and *SSCerr*

SSC Deck

TITLE

SSC cell lattice - 14 SSC arc cells w/ concatenated bends

SBEND, B01, L = 5 * 17.34, ANGLE = 5 * 17.34 / 10108.0, K2 = 0.0

SBEND, B02, L = 5 * 17.34, ANGLE = 5 * 17.34 / 10108.0, K2 = 0.0

SBEND, B03, L = 5 * 17.34, ANGLE = 5 * 17.34 / 10108.0, K2 = 0.0

SBEND, B04, L = 5 * 17.34, ANGLE = 5 * 17.34 / 10108.0, K2 = 0.0

⋮

SBEND, B27, L = 5 * 17.34, ANGLE = 5 * 17.34 / 10108.0, K2 = 0.0

SBEND, B28, L = 5 * 17.34, ANGLE = 5 * 17.34 / 10108.0, K2 = 0.0

QUAD, QF, L = 3.32, K1 = 0.003178

QUAD, QD2, L = 1.66, K1 = -0.003178

SEXT, SF, L = 1.5, K2 = 0.00987 / 1.5

SEXT, SD, L = 1.5, K2 = -0.01591 / 1.5

DRIFT, END, L = 0.4

DRIFT, BPM, L = 0.2

DRIFT, DSP, L = 3.48

LINE, CELL (BB1, BB2) = (QD2, END, BPM, &
 SD, DSP, &
 BB1, &
 END, QF, END, BPM, &
 SF, DSP, &
 BB2, &
 END, QD2)

LINE, CELL14 = (CELL(B01, B02), CELL(B03, B04), CELL(B05, B06), &
 CELL(B07, B08), CELL(B09, B10), CELL(B11, B12), &

CELL(B13, B14), CELL(B15, B16), CELL(B17, B18), &
CELL(B19, B20), CELL(B21, B22), CELL(B23, B24), &
CELL(B25, B26), CELL(B27, B28))

CELL, CELL14

VARY, QD2[K1], STEP = 1.E-6

VARY, QF[K1], STEP = 1.E-6

CONSTRAI, #E, MUX = 2.265, MUY = 2.285

MIGRAD

ENDMATCH

USE, CELL14

PRINT, CELL14[1]

TWISS, LINE = CELL14, TAPE

STOP

SSCerr Deck

TITLE

SSCerr cell lattice with bend errors: Ave=2.520e-5 Rms=1.873e-4

SBEND, B01, L = 5 * 17.34, ANGLE = 5 * 17.34 / 10108.0, K2 = 6.0754E-5

SBEND, B02, L = 5 * 17.34, ANGLE = 5 * 17.34 / 10108.0, K2 = -2.5014E-4

SBEND, B03, L = 5 * 17.34, ANGLE = 5 * 17.34 / 10108.0, K2 = 1.5957E-5

SBEND, B04, L = 5 * 17.34, ANGLE = 5 * 17.34 / 10108.0, K2 = -2.1917E-4

SBEND, B05, L = 5 * 17.34, ANGLE = 5 * 17.34 / 10108.0, K2 = 1.7396E-4

SBEND, B06, L = 5 * 17.34, ANGLE = 5 * 17.34 / 10108.0, K2 = 2.1660E-5

SBEND, B07, L = 5 * 17.34, ANGLE = 5 * 17.34 / 10108.0, K2 = -4.3307E-4

SBEND, B08, L = 5 * 17.34, ANGLE = 5 * 17.34 / 10108.0, K2 = -1.5193E-4

SBEND, B09, L = 5 * 17.34, ANGLE = 5 * 17.34 / 10108.0, K2 = 7.0427E-5

⋮
⋮

SBEND, B24, L = 5 * 17.34, ANGLE = 5 * 17.34 / 10108.0, K2 = -9.8915E-5

SBEND, B25, L = 5 * 17.34, ANGLE = 5 * 17.34 / 10108.0, K2 = 1.1680E-4

SBEND, B26, L = 5 * 17.34, ANGLE = 5 * 17.34 / 10108.0, K2 = -1.0955E-4

SBEND, B27, L = 5 * 17.34, ANGLE = 5 * 17.34 / 10108.0, K2 = -1.1175E-4

SBEND, B28, L = 5 * 17.34, ANGLE = 5 * 17.34 / 10108.0, K2 = 1.2723E-4

<The rest of the deck is the same as the SSC deck.>

Note MAD vers 6.0 allows one to generate random error fields for various magnets during the run rather than externally as we did.

APPENDIX C

Calculation of I_{31} , I_{32} , and I_{33} Integrals

When implementing the tracking algorithm, described in Section 4, integrals of the forms I_{31} , I_{32} , and I_{33} , Eqs. (4.4), (4.10), and (4.11) respectively, must be calculated. These integrals depend upon the parameters $b_2(s)$, $\beta_x(s)$, $\beta_y(s)$, $\psi_x(s)$, and $\psi_y(s)$ which are specified by the configuration of the ring lattice. We pass this information to the program in the form of a table of Twiss parameters. Accelerator programs, such as MAD,¹² are used to generate such a table for a specific configuration. Initially, the integrals are calculated over each individual magnet and saved in a file. When tracking, the ring is subdivided into steps, containing one or more magnets, to reduce errors. The integrals over each magnet are then added together to form integrals over the steps. The coefficients of the series for $G^{(1)}$ and $G^{(2)}$, Eqs. (4.3) and (4.8), are calculated from these integrals. Because the coefficients are periodic they only need to be calculated once for each step.

Once the lattice is specified, the integrals are calculated numerically over each individual magnet, taking each magnet to be a single step about the ring. If a magnet has zero length, the strength parameter b_2 is assumed to be the integrated strength and the integral is set equal to the integrand. Otherwise, Simpson's 1/3 integration rule is used:

$$\begin{aligned}
 I_{31}(s_f, s_i) &= \int_{s_i}^{s_f} f(s_f, s) ds \\
 &= \frac{\Delta s}{3} [f(s_f, s_i) + 4f(s_f, s_1) + 2f(s_f, s_2) + \cdots \\
 &\quad + 2f(s_f, s_{n-2}) + 4f(s_f, s_{n-1}) + f(s_f, s_f)] + O(\Delta s^4)
 \end{aligned} \tag{C1}$$

where

$$\Delta s = \frac{s_f - s_i}{N}; \quad s_1 = s_i + \Delta s; \quad \cdots$$

Note that the integrand contains a phase factor which depends upon the final point of the step, s_f . The values of $\beta(s)$ and $\psi(s)$ are calculated from the values of β , α , and ψ at the end of the magnet, $s = s_f$, using the expression for the

drift space beta function:

$$\begin{aligned}\beta(s) &= \beta_f - 2\alpha_f(s - s_f) + \left[\frac{1 + \alpha_f^2}{\beta_f} \right] (s - s_f)^2 \\ \psi(s) &= \psi_f + \tan^{-1} \left[\frac{(s - s_f)}{\beta_f - \alpha_f(s - s_f)} \right]\end{aligned}\tag{C2}$$

where $\alpha(s) = -\beta'(s)/2$ and β_f , α_f , and ψ_f are the β , α , and ψ values at $s = s_f$. The expression for the horizontal beta function in a bending magnet is

$$\begin{aligned}\beta(s) &= \beta_f - \alpha_f \rho \sin(2(s - s_f)/\rho) + \left[\left(\frac{1 + \alpha_f^2}{\beta_f} \right) \rho^2 - \beta_f \right] \sin^2((s - s_f)/\rho) \\ \psi(s) &= \psi_f + \tan^{-1} \left[\frac{\rho \sin((s - s_f)/\rho)}{\beta_f \cos((s - s_f)/\rho) - \alpha_f \rho \sin((s - s_f)/\rho)} \right]\end{aligned}\tag{C3}$$

where ρ is the bending radius. The vertical beta function behaves as if in a drift.

The forms of the I_{32} and I_{33} integrals are similar to the single integrals, and they are evaluated in the same manner. The intermediate values of I_{31} , needed when evaluating the integrands, are calculated using Simpson's 1/3 rule and a single panel three point rule:

$$\begin{aligned}I_{31}(s_1, s_0) &= \int_{s_0}^{s_1} f(s_f, s) ds \\ &= \frac{\Delta s}{12} [5f(s_f, s_0) + 8f(s_f, s_1) - f(s_f, s_2)] + O(\Delta s^4)\end{aligned}\tag{C4}$$

where

$$\Delta s = s_1 - s_0 = s_2 - s_1.$$

Note that the integrand still depends upon s_f , the final point in the step, although the limits of the integral are s_i and s_1 .

The integrals are stored in arrays as they are calculated and then written to a file for subsequent retrieval. There are ten I_{31} integrals, one hundred I_{32} integrals, and one hundred and seventy-five I_{33} integrals to be calculated for each sextupole magnet. Note that although only fifty-four I_{32} integrals are needed to calculate the coefficients, others are needed when combining the I_{33} integrals into steps. The speed of access is not of concern for the integrals, they are only accessed to calculate the coefficients of the series for $G^{(1)}$ and $G^{(2)}$, and so a simple indexing method is used.

In the case of the sextupole perturbation there are only ten possible values for the three parameter group (n, m_x, m_y) : $(1,-1,-2)$, $(1,-1,0)$, $(1,-1,2)$, $(1,1,-2)$, $(1,1,0)$, $(1,1,2)$, $(3,-3,0)$, $(3,-1,0)$, $(3,1,0)$, $(3,3,0)$. A unique index between 0 and 9 is found from:

$$Index(n, \mathbf{m}) = \frac{n(5 - m_x) + 4m_x + m_y}{2} \quad (C5)$$

This scheme leads to 100 spaces per magnet for the double integrals and 1000 for the triple. Additional space is saved when storing the triple integrals by using a one dimensional array 1000 elements long to convert the initial index, a value between 0 and 999, to an index between 1 and 175.

The ring is subdivided into steps to reduce the errors when tracking. The integrals which were initially calculated over the individual magnets, must be combined to form integrals over the steps. Unfortunately, the combining is complicated by the phase factor, $e^{-i\mathbf{m} \cdot \boldsymbol{\psi}(s_f)}$, appearing in the integrands. The integrals are combined using the recursive relations:

$$I_{31}(\mathbf{p}, s_n, s_0) = I_{31}(\mathbf{p}, s_n, s_{n-1}) + e^{i\mathbf{m} \cdot [\boldsymbol{\psi}(s_{n-1}) - \boldsymbol{\psi}(s_n)]} I_{31}(\mathbf{p}, s_{n-1}, s_0) \quad (C6)$$

$$I_{32}(\mathbf{p}, \mathbf{p}', s_n, s_0) = I_{32}(\mathbf{p}, \mathbf{p}', s_n, s_{n-1}) + e^{i(\mathbf{m} + \mathbf{m}') \cdot [\boldsymbol{\psi}(s_{n-1}) - \boldsymbol{\psi}(s_n)]} I_{32}(\mathbf{p}, \mathbf{p}', s_{n-1}, s_0) + e^{i\mathbf{m}' \cdot [\boldsymbol{\psi}(s_{n-1}) - \boldsymbol{\psi}(s_n)]} I_{31}(\mathbf{p}, s_n, s_{n-1}) I_{31}(\mathbf{p}', s_{n-1}, s_0) \quad (C7)$$

$$I_{33}(\mathbf{p}, \mathbf{p}', \mathbf{p}'', s_n, s_0) = I_{33}(\mathbf{p}, \mathbf{p}', \mathbf{p}'', s_n, s_{n-1}) + e^{i(\mathbf{m} + \mathbf{m}' + \mathbf{m}'') \cdot [\boldsymbol{\psi}(s_{n-1}) - \boldsymbol{\psi}(s_n)]} I_{33}(\mathbf{p}, \mathbf{p}', \mathbf{p}'', s_{n-1}, s_0) + e^{i\mathbf{m}' \cdot [\boldsymbol{\psi}(s_{n-1}) - \boldsymbol{\psi}(s_n)]} I_{32}(\mathbf{p}, \mathbf{p}'', s_n, s_{n-1}) I_{31}(\mathbf{p}', s_{n-1}, s_0) + e^{i\mathbf{m}'' \cdot [\boldsymbol{\psi}(s_{n-1}) - \boldsymbol{\psi}(s_n)]} I_{32}(\mathbf{p}, \mathbf{p}', s_n, s_{n-1}) I_{31}(\mathbf{p}'', s_{n-1}, s_0) + e^{i(\mathbf{m}' + \mathbf{m}'') \cdot [\boldsymbol{\psi}(s_{n-1}) - \boldsymbol{\psi}(s_n)]} \times I_{31}(\mathbf{p}, s_n, s_{n-1}) I_{31}(\mathbf{p}', s_{n-1}, s_0) I_{31}(\mathbf{p}'', s_{n-1}, s_0) \quad (C8)$$

where $I(s_1, s_0)$ is an integral over the first magnet, etc. These values are then used to calculate the coefficients for the $G^{(1)}$ and $G^{(2)}$ summations, Eqs. (4.3) and (4.8).

APPENDIX D

CALCULATION OF INVARIANTS IN FIRST ORDER PERTURBATION THEORY

The goal when calculating invariant curves, is to find surfaces in phase space which are invariant over time. This is done by solving for a transformation which leaves the Hamiltonian as a function of the action only. From Hamilton's equations, the action is then a constant of the motion. The invariant surfaces can be found as a function of the constant action by reversing the transformation. For a review of this technique see Ref. 4.

Suppose that the problem is described by a Hamiltonian of the form:

$$H = H_0(\mathbf{J}) + V(\phi, \mathbf{J}, \theta) , \quad (\text{D1})$$

where $V(\phi, \mathbf{J}, \theta)$ is periodic in ϕ and θ , and has a zero average with respect to them:

$$\int_0^{2\pi} d\theta \int_0^{2\pi} d\phi V(\phi, \mathbf{J}, \theta) = 0 . \quad (\text{D2})$$

If V has a non-zero average, the average can be absorbed into H_0 .

Similar to the case of superconvergent tracking, we use canonical transformations to remove the perturbation to first order. The generating function, which we will denote by \mathcal{G} , must be periodic in θ . The new Hamiltonian is given by:

$$H_1 = H_0(\mathbf{J}_1 + \mathcal{G}_\phi) + V_0(\phi, \mathbf{J}_1 + \mathcal{G}_\phi, \theta) + \mathcal{G}_\theta , \quad (\text{D3})$$

where the new variables, ϕ_1 and \mathbf{J}_1 , are calculated from \mathcal{G} using Eqs. (2.3) and (2.4). H_1 can be re-written as:

$$\begin{aligned} H_1 = & H_0(\mathbf{J}_1) + \nu_{\mathbf{J}_1}(\mathbf{J}_1) \mathcal{G}_\phi^2 / 2 + \dots \\ & + [\nu(\mathbf{J}_1) \mathcal{G}_\phi + \mathcal{G}_\theta + V(\phi, \mathbf{J}_1, \theta)] \\ & + [V(\phi_0, \mathbf{J}_1 + \mathcal{G}_\phi, \theta) - V(\phi, \mathbf{J}_1, \theta)] , \end{aligned} \quad (\text{D4})$$

where $\nu(\mathbf{J}_1)$ is the tune of the unperturbed problem: $\partial H_0(\mathbf{J}_1) / \partial \mathbf{J}_1$. If the expression in the first bracket is set to zero the new perturbation will be of order

ϵ^2 . Since both \mathcal{G} and V are periodic in ϕ_0 , they can be Fourier analyzed, and the equations for the Fourier coefficients of \mathcal{G} are:

$$i\mathbf{m} \cdot \boldsymbol{\nu}(\mathbf{J}_1)g_{\mathbf{m}} + \frac{\partial g_{\mathbf{m}}}{\partial \theta} + v_{\mathbf{m}} = 0. \quad (\text{D5})$$

These equations are identical to the equations for $G^{(1)}$, except we will look for solutions periodic in θ , rather than one which goes to 0 as $\theta \rightarrow \theta_0$. The periodic solution for $g_{\mathbf{m}}$ is:

$$g_{\mathbf{m}}(\mathbf{J}_1, \theta) = \frac{i}{2 \sin \pi \mathbf{m} \cdot \boldsymbol{\nu}} \int_{\theta}^{\theta+2\pi} e^{i\mathbf{m} \cdot \boldsymbol{\nu}(\theta' - \theta - \pi)} v_{\mathbf{m}}(\mathbf{J}_1, \theta') d\theta'. \quad (\text{D6})$$

where $g_{\mathbf{m}}$ and $v_{\mathbf{m}}$ are the \mathbf{m} th coefficients of the Fourier series for \mathcal{G} and V in ϕ_0 .

Now the new Hamiltonian becomes:

$$\begin{aligned} H_1 &= H_0(\mathbf{J}_1) + [V_{\mathbf{J}_1} \cdot \mathcal{G}_{\phi_0} + \mathcal{G}_{\phi_0} \cdot \boldsymbol{\nu}_{\mathbf{J}_1} \cdot \mathcal{G}_{\phi_0}/2] + \dots \\ &\equiv H_0(\mathbf{J}_1) + V'(\phi_1, \mathbf{J}_1, \theta). \end{aligned} \quad (\text{D7})$$

It is a function of \mathbf{J}_1 to first order. As in the case of superconvergent tracking, we can now return to Eq. (D1), and repeat the process. After n steps, the Hamiltonian will be a function of \mathbf{J}_n plus a perturbation of order ϵ^{2^n} and the action, \mathbf{J}_n , will be a constant plus an error of order ϵ^{2^n} . By reversing the transformation, the invariant surfaces can be calculated from a given \mathbf{J}_n with an error $O(\epsilon^{2^n})$.

The form of \mathcal{G}_1 is very similar to that of $G^{(1)}$. Using Eq. (D6) \mathcal{G}_1 is:

$$\begin{aligned} \mathcal{G}_1 &= -\frac{\sqrt{8}}{48} J_x^{\frac{3}{2}} [e^{3i\phi_x} I'_{31}(3, 3, 0) + 3e^{i\phi_x} I'_{31}(3, 1, 0) + \text{CC}] \\ &+ \frac{\sqrt{8}}{16} J_x^{\frac{1}{2}} J_y [e^{i(\phi_x + 2\phi_y)} I'_{31}(1, 1, 2) + 2e^{i\phi_x} I'_{31}(1, 1, 0) \\ &+ e^{i(\phi_x - 2\phi_y)} I'_{31}(1, 1, -2) + \text{CC}]. \end{aligned} \quad (\text{D8})$$

where

$$I'_{31}(n, \mathbf{m}, s_i) = \frac{i}{2 \sin \pi \mathbf{m} \cdot \boldsymbol{\nu}} \int_{s_i}^{s_i+2\pi} b_2 \beta_x^{\frac{n}{2}} \beta_y^{\frac{3-n}{2}} e^{i\mathbf{m} \cdot [\boldsymbol{\psi}(s') - \boldsymbol{\psi}(s_i) - \boldsymbol{\nu}\pi]} ds'. \quad (\text{D9})$$

Using the definition of the tune, ν : $2\pi\nu \equiv \psi_i(C) = \int_0^C ds'/\beta_i(s')$, where C is the

circumference of the ring, I'_{31} can be written in terms of I_{31} (Eq. (4.4)):

$$I'_{31}(n, \mathbf{m}, s_i) = \frac{ie^{i\pi\mathbf{m}\cdot\nu}}{2\sin\pi\mathbf{m}\cdot\nu} I_{31}(n, \mathbf{m}, s_i + C) . \quad (\text{D10})$$

Thus the integrals needed can be easily calculated from results which we already have.

To calculate the invariant curves, the 'invariant' action is solved for implicitly from the initial conditions in the (ϕ_0, \mathbf{J}_0) phase space:

$$\mathbf{J}_1 = \mathbf{J}_i - \mathcal{G}_\phi(\phi_i, \mathbf{J}_1, s_i + C) . \quad (\text{D11})$$

From Hamilton's equations, \mathbf{J}_1 is invariant with an error of order ϵ^2 . The invariant curve is plotted by varying ϕ and calculating \mathbf{J}_0 :

$$\mathbf{J}_0 = \mathbf{J}_1 + \mathcal{G}_\phi(\phi_0, \mathbf{J}_1, s_i + C) + O(\epsilon^2) . \quad (\text{D12})$$

REFERENCES

1. F.C. Iselin, in: *Nonlinear Dynamics Aspects of Particle Accelerators*, Lecture Notes in Physics, vol. 247 (Springer, Berlin, 1986).
2. A. Wrulich, *ibid.*
3. R.V. Servranckx, IEEE Trans. Nucl. Sci. NS-32 (1985) 2186.
4. R. D. Ruth, *Single Particle Dynamics in Circular Accelerators*, AIP Conf. Proc. 153 (1987) 150.
5. R. L. Warnock and R. D. Ruth, *Invariant Tori Through Direct Solution of the Hamilton-Jacobi Equation*, Physica 26D (1987) 1.
6. K. Brown, F. Rothacker, D. Carey, and C. Iselin, *TRANSPORT: A Computer Program for Designing Charged Particle Beam Transport Systems*, SLAC-91 Rev. 2, 1977.
7. R.D. Ruth, IEEE Trans. on Nucl. Sci. NS-30 (1983) 2669.
8. R. D. Ruth, T. Raubenheimer, R.L. Warnock, *Superconvergent Tracking and Invariant Surfaces in Phase Space*, IEEE Trans. Nucl. Sci. NS-32 (1985) 2206.
9. H. Goldstein, *Classical Mechanics*, Addison-Wesley, 1980.
10. A.C. Hearn, REDUCE vers. 3.1, The Rand Corporation, Santa Monica CA.
11. A.C. Hindmarsh and G.D. Byrne, EPSODE, Lawrence Livermore Laboratory, June 1975.
12. F.C. Iselin and J. Niederer, THE MAD PROGRAM (Methodical Accelerator Design vers. 4.0), CERN/LEP-TH/87-33.
13. M.D. Woodley, M.J. Lee, J. Jäger and A.S. King, IEEE Trans. Nucl. Sci. NS-30 (1983) 2367.
14. All SSC parameters were taken from: *SSC Conceptual Design Parameter List*, SSC Central Design Group, Lawrence Berkeley Laboratory, March 1986, SSC-SR-2020A.
Note that the current design differs slightly.